Department of Electrical and Computer Systems Engineering

Technical Report
MECSE-26-2003

Uncertainty of Line Segments Extracted from Static SICK PLS Laser Scans

A. Diosi and L. Kleeman

MONASH UNIVERSITY

Uncertainty of Line Segments Extracted from Static SICK PLS Laser Scans

Albert Diosi and Lindsay Kleeman
Intelligent Robotics Research Centre
Department of Electrical and Computer Systems Engineering
Monash University, Clayton, VIC 3168, Australia
{Albert.Diosi,Lindsay.Kleeman}@eng.monash.edu.au

November 12, 2003

Abstract

Data fusion using Kalman filters requires reasonably good error models. Our intention to fuse line segments, corners and edges obtained from a laser scanner and from advanced sonars provided the motivation on the investigation of Sick PLS laser scanner range measurement reliability, and line segment estimation precision. We present an approach for fitting lines straight in the lasers polar coordinate system, which enables a simple estimation of line parameter covariance. We also develop systematic error models for line parameter estimation. Finally we measure our systematic and random error models experimentally, and show, that systematic errors can be larger than random ones.

Contents

1 Introduction

The motivation for the work behind this technical report is our aim to perform simultaneous localization and mapping (SLAM) by fusing data from advanced sonars and a laser range finder.

The advanced sonars mounted on our robot Slambot are not just capable of measuring range and bearing of objects with excellent precision [10] ($\sigma_{bearing} \approx 0.1°$ and $\sigma_{range} \approx 0.2\ mm$), but they are also capable of classifying objects as planes, corners or edges.

Slambots laser scanner is a SICK PLS101-112. Contrary to the common belief, measurements obtained of an object using this particular sensor are in general less precise, than that of advanced sonar. We are planning to perform sensor fusion in a Kalman filter fashion, i.e. by weighting measurements according to their error estimate. Therefore it is essential for us to know how accurate are lines estimated from laser scans. To estimate the uncertainty in the line parameters, it is necessary to find out how precise are the range measurement of the laser.

By looking at the method of range measurement, there are 3 major laser scanners types [6]: Amplitude Modulated Continuous Wave lasers, time-of-flight lasers and Frequency Modulated Continuous Wave lasers. We are interested only in time-of-flight lasers like the PLS, because different principles of operation might introduce different types of errors.

When characterizing a laser scanner, researchers among others look at the following properties (as in [14][18]): the dependence of range error on the distance of the object, orientation of the object, surface properties of the object and operation time. When measuring the effect of distance and target plane angle on accuracy, usually a special calibration tool is used which contains a target plane which can be translated along one axis and rotated around another axis either manually [14] or through automatic control [18]. In paper [14] for a time-of-flight laser scanner manufactured by Schwartz Electro-optics Inc., and in [18] for a Sick LMS 200 laser scanner, the authors measured a range error depending on distance.

In [14], they report that range error increases with increasing angle between target plane normal and laser beam. In [18], the error changes with the incidence angle but instead of growing monotonously, it gets smaller after $30°$. There is neither an explanation nor a qualitative description for these behaviors in these papers. In both papers, targets with different surface properties were tested and the general conclusion was that the reflectivity of the target had a more significant effect on the range error than color.

According to both papers, a range error drift of both lasers was observed during warm-up.

Even though the existence of systematic errors in laser scanners is known, their effect in feature extraction or scan matching is often neglected. A rare example for the opposite can be found in [13], where the authors analyzed the effect of bias in range measurements on position estimates resulting from scan matching.

The effect of systematic and non-systematic errors in the range readings on estimated line parameters depends on the line fitting method. There are several approaches for line fitting used. In [11], a local Cartesian coordinate system is placed into the center of gravity of a line segment, with the vertical axis pointing in the opposite direction, than that of the laser. The regression coefficient of the line is determined by linear regression, which is sensitive to noise for vertical lines. From the knowledge of the center of gravity and the regression coefficient the angle and perpendicular distance parameters of the normal form of a line are calculated. The covariance of the angle and distance estimate of the line is derived, under the assumption of error free laser bearings.

The author in [8] uses the solution given in [3], where the angle and distance parameters of a line are estimated by minimizing the sum of square perpendicular distances of the points from the line in Cartesian coordinate system. A simple covariance estimate is given of the line parameters, assuming uniform covariance of each point. However this assumption is only valid for short line segments if data is obtained from a laser range finder utilizing a rotating mirror.

Similarly to [8] in [1] the authors minimized the sum of square perpendicular distances of points to a line in Cartesian coordinate system, however their solution accounts for nonuniform weights of points. They also show an equivalent solution with polar coordinates, which was used to derive a line parameter covariance estimate assuming only errors in the range measurements.

Contrary to the previously described methods, in [15] the authors take advantage of the description of a line in polar coordinate system, and minimize the sum of square errors of reciprocal ranges. However we believe that due to the use of the reciprocal of the range, their approach implicitly weights closer points more than further ones.

In all of these papers, systematic errors are neglected in line estimates, and little experimental evidence is presented to support error models. Systematic errors are shown in this report to be a significant component of the final errors in line parameters for the Sick PLS.

In this report we develop an approach for fitting lines straight in polar coordinate system which enables simple covariance estimation. Then we describe the results of experiments aimed at determining the influence of several factors on the PLS range systematic errors. The results are used to derive systematic error models which describe how the factors influence systematic errors in line estimates. Finally experimental validation of the constructed systematic and non-systematic error models is undertaken.

2 Laser Line Error Model

2.1 Specifications of the SICK PLS Laser Sensor

Probably two of the most common laser scanners mounted on mobile robots are the SICK PLS (see fig. 1) and the newer LMS. In this report only the PLS 101-112 version is going to be dealt with.

A rotating mirror inside the PLS sensor deflects an infrared laser beam in the range from $0°$ to $180°$ [4]. Distance is determined by measuring the time of flight of the

Figure 1: SICK PLS101-112 laser range finder.

emitted laser pulses. The resolution of the sensor is 5 cm in the distance, and maximally $0.5°$ in the angles. The worst case error according to [4] is 94 mm at the distance of 2 m and 131 mm at 4 m. One $180°$ scan takes 40 ms to complete. The maximum range of the sensor is 50 m. Measurements from the sensor are transmitted to a PC through a serial line. The LMS sensor is an improved version of the PLS. Its angular resolution has been reduced to $0.25°$. Its distance resolution has been reduced to 1 cm. Due to the improved capabilities of the LMS sensor, the error models developed here for the PLS may not be applicable for the LMS sensor.

The patent [17] of the Deutches Patent Amt describes the operation of a laser range finder, which is very similar to the PLS. Therefore we assume, that the PLS and the patent [17] are related. The laser range finder described in [17] works the following way: A laser source sends out a pulse of 3.5 ns duration and a counter of 330 ps resolution is started. The 330 ps time resolution results in 5 cm distance resolution. The returned pulse is detected by a photo receiver. The output from the receiver is fed into a comparator. When the received signal is 7 times larger than the average noise level of the photo receiver, then the output of the comparator stops the counter. Comparing the output of the photo receiver with multiples of the average noise level measured on the photo receiver helps to keep false detection rate low.

Returning light pulses with different light intensities generate signals on the photo detector with different rise times. In an example from [17], the change in the rise time generates a 20 cm error in the range measurement. To correct for this error, a peak detector consisting of ECL comparators is employed to discriminate between 6 levels. The output of the peak detector is fed into a microprocessor, where the time of flight is compensated for the rise time error. However as we will show later, the 6 level resolution results in easily detectable errors.

The following factors with a possible influence on the precision of line segment parameters measured by the laser have been identified:

1. Random errors in the range measurements.

2. Bias in the range quantization error.

3. Bias changing with the incidence angle of laser beam and target surface.

4. Constant bias in the range measurements.

5. Range bias growing with distance.

6. Laser plane misaligned with the floor.

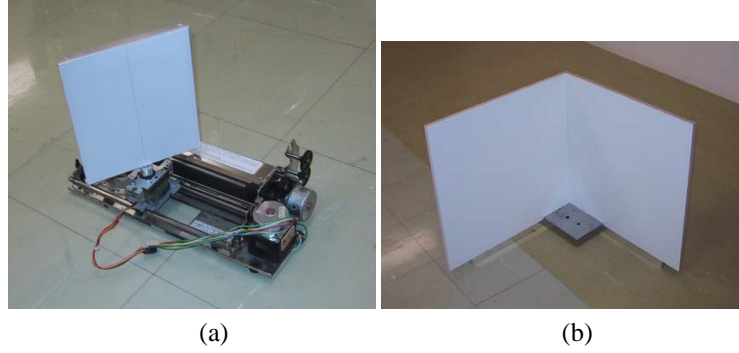7. Error in the laser beam bearings.

4

Figure 2: Laser calibration tool made from old printer a), "perfect" corner b).

In the following subsections, we will focus on most of the above mentioned error sources and discuss their contribution to the overall error. In this work, errors due to imprecise laser beam bearings are not considered.

2.2 Laser Calibration Tools

For evaluation of the line error models and for testing of the Sick PLS, two tools were used. The first tool resembles a perfect right angle corner with 60 cm long arms (see fig. 2b). The angle of the corner was estimated as $89.85° \pm 0.3°$ the following way: Tape measure was used to measure the length of the arms and the hypotenuse. Then the cosine law was applied to calculate the opening angle of the corner. The error bounds were obtained by assuming ± 1 mm error in the measurements. The surface of the corner has a rather shiny finish with visible specular reflections.

The inspiration for the second tool used came from [18], where the authors used a 4 m linear motion table with a rotating target plane mounted on it. We created a similar, but inexpensive setup (see fig. 2a), by recycling the head moving mechanism of a discarded printer. We replaced the head with a 16x16 cm target plane rotated by a stepper motor from a 5.25" floppy drive. The target planes surface was covered with thick, white, non-glossy paper. The mechanism was controlled by a PC running Linux. The achieved resolution in distance and angle was 0.3 mm and $1.8°$.

2.3 Line Representation and Identification

The normal form representation of a line is described by the following equation in a Cartesian coordinate system (X, Y) (see fig. 3a):

$$x \cos(\alpha) + y \sin(\alpha) = d \tag{1}$$

where α is the angle between the X axis and the normal of the line, and $d \geq 0$ is the perpendicular distance of the line to the origin. However, x and y are a function of the angle of the laser beam (ϕ) and the measured range (r). Therefore it is often more convenient to work with a line in the laser range finder's polar coordinate system (Φ, R) (see fig. 3b), where a line is represented with the well known equation (see appendix A.1 for derivation):
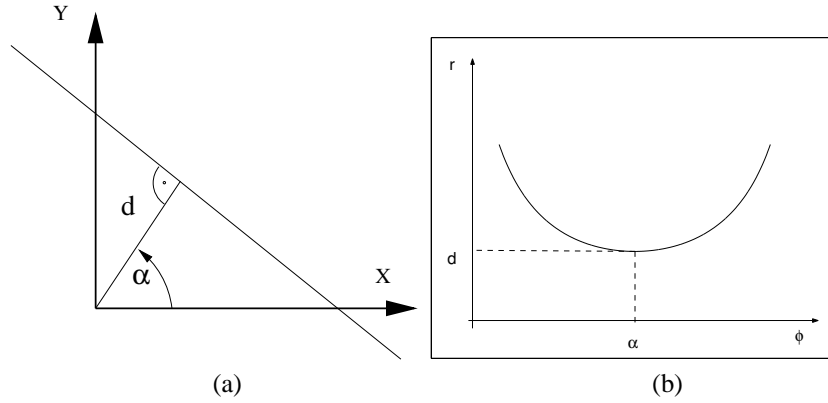
$$r = \frac{d}{\cos(\alpha - \phi)} \tag{2}$$

5

Figure 3: Line in Cartesian (X, Y) and in polar (R, Φ) coordinate system.

As it can be seen from fig. 3b, the curve representing a line is uniquely described with the coordinates of its minimum (α, d).

To identify the parameters of a line from measured data points, several approaches can be used. For example, the equations for linear regression (eq. 4-5) can be used to determine the parameters of a line in slope-intercept form (eq. 3) and then convert the resulting line into normal form using eq. 6-7 (see appendix A.2). E.g:

$$y = kx + q \tag{3}$$

where,

$$k = \frac{n \sum x_i y_i - (\sum x_i)(\sum y_i)}{n \sum x_i^2 - (\sum x_i)^2} \tag{4}$$

$$q = \frac{\sum y_i - k \sum x_i}{n} \tag{5}$$

Then use

$$\alpha = \arccos \frac{-k}{\sqrt{1 + k^2}} + (\text{sign}(q) - 1)\frac{\pi}{2} \tag{6}$$

$$d = \frac{|q|}{\sqrt{1 + k^2}} \tag{7}$$

The drawbacks of the above mentioned approach are the following:

1. For vertical lines the results are imprecise due to numerical instability resulting from small numbers in the denominator of eq. 4.

2. The cost function being minimized doesn't reflect the way the data points were collected. The points being processed in (X, Y) are the result of a nonlinear transformation of points from (Φ, R) what makes errors in the x and y coordinates correlated. Due to the cost function, not the sum of squared distances of points from the line is minimized, but the sum of square errors in y coordinates. Thus errors in x coordinates are not regarded.

3. For us the derivation of a covariance estimate for (k, q) based upon the uncertainty in (ϕ, r) is not really simple.

6

However, for horizontal lines with no random noise in the range, the above mentioned method works fine, therefore we will use it later due to its simplicity for the derivation of some results.

A better approach than the previous one is to minimize the sum of square perpendicular distances of points from lines (see appendix A.3). However, we developed an approach for finding out (α, d) with its estimated uncertainty directly in (Φ, R) coordinate system for the price of linearization.

If we linearize eq. 2 around (α_0, d_0), we get

$$r_i - r_{0i} \approx \frac{d_0 \sin(\alpha_0 - \phi_i)}{\cos^2(\alpha_0 - \phi_i)}\Delta\alpha + \frac{1}{\cos(\alpha_0 - \phi_i)}\Delta d \tag{8}$$

This is restated in vector form as

$$\mathbf{\Delta r} = \mathbf{r_m} - \mathbf{r_0} = \mathbf{H_0}\mathbf{\Delta b} + \mathbf{R} \tag{9}$$

Where

$$\mathbf{H_0} = \begin{bmatrix} \cdots & \cdots \\ \frac{d_0 \sin(\alpha_0 - \phi_i)}{\cos^2(\alpha_0 - \phi_i)} & \frac{1}{\cos(\alpha_0 - \phi_i)} \\ \cdots & \cdots \end{bmatrix} \tag{10}$$

$$\mathbf{\Delta b} = \begin{bmatrix} \Delta\alpha & \Delta d \end{bmatrix}^T \tag{11}$$

$\mathbf{R}$ is a vector of measurement noise with a covariance matrix $\sigma_r^2 I$, $\mathbf{r_m}$ is a vector containing measured ranges and $\mathbf{r_0}$ is a vector representing ranges estimated using (α_0, d_0).

Using the common linear regression (see [16]) iteratively on the linearized problem (eq. 8), we can find (α, d) which minimizes the square sum of range residuals, the following way:

$$\mathbf{r_j} = \begin{bmatrix} r_{j1} & \cdots & r_{ji} & \cdots & r_{jn} \end{bmatrix}^T =$$
$$= \begin{bmatrix} \cdots & \frac{d_j}{\cos(\alpha_j - \phi_i)} & \cdots \end{bmatrix}^T \tag{12}$$

$$\mathbf{H_j} = \begin{bmatrix} \cdots & \cdots \\ \frac{d_j \sin(\alpha_j - \phi_i)}{\cos^2(\alpha_j - \phi_i)} & \frac{1}{\cos(\alpha_j - \phi_i)} \\ \cdots & \cdots \end{bmatrix} \tag{13}$$

$$\mathbf{\Delta b} = \left(\mathbf{H_j^T H_j}\right)^{-1} \mathbf{H_j^T}(\mathbf{r_m} - \mathbf{r_j}) \tag{14}$$

$$\begin{bmatrix} \alpha_{j+1} \\ d_{j+1} \end{bmatrix} = \begin{bmatrix} \alpha_j \\ d_j \end{bmatrix} + \mathbf{\Delta b} \tag{15}$$

Eq. 14 yields the least squares estimate, and can be found for example in [9]. By initializing $\mathbf{r_j}$ with (α_0, d_0) obtained from either eq. 4-7, or from minimizing the perpendicular distance of points from the line (see eq. 132-133), this iterative process converges quickly. The advantage of the above mentioned approach is that a simple covariance estimate is obtained due to the use of linear regression [16]:

$$cov(\mathbf{\Delta b}) = cov(\alpha, d) = \sigma_r^2 (\mathbf{H^T H})^{-1} \tag{16}$$

where the noise in the range measurements is assumed to be zero mean white noise with a variance of σ_r^2. However the noise is correlated as will be seen in results below. The use of eq. 16 also assumes that there is no error in the measurement of ϕ_i.
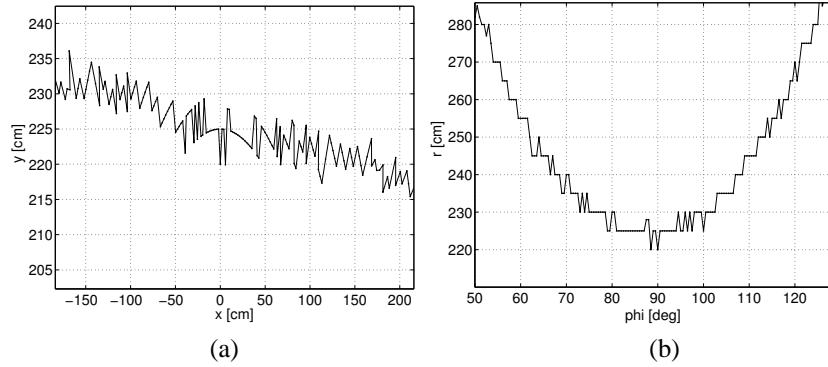
Figure 4: Laser scan of a line in Cartesian (X, Y) and in polar (R, Φ) coordinate system.
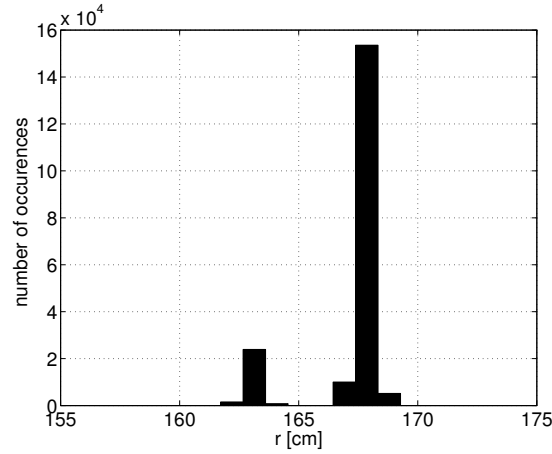

Figure 5: Distribution of laser measurements of one point of a wall.

2.4   Errors Due to Quantization and Random Noise

Figure 4a shows a laser scan of a wall in (X, Y) coordinate system. The arc shapes in the figure are the results of range quantization as it can be better seen in (Φ, R) coordinate system (fig. 4b). Even though a 5 cm quantization step can be observed most of the time, there are some readings, which are between 2 quantization levels. Furthermore, from time to time, all range measurements shift randomly by ± 1 cm for the duration of one scan. This is depicted on fig. 5 which shows a distribution of 200k samples taken of the same point. The small bars on both sides of the main peaks demonstrate this 1 cm shift. Judging from the results of other experiments, it seems, that the 1 cm shift occurs with roughly the same probability in both directions. Since the shift occurs for all measurements of a particular scan, we categorize this error as a bias shift, and will deal with it later.

For our statistical analysis of the quantization error we approximate the measurement process with the following model: to the true range r' zero mean white Gaussian
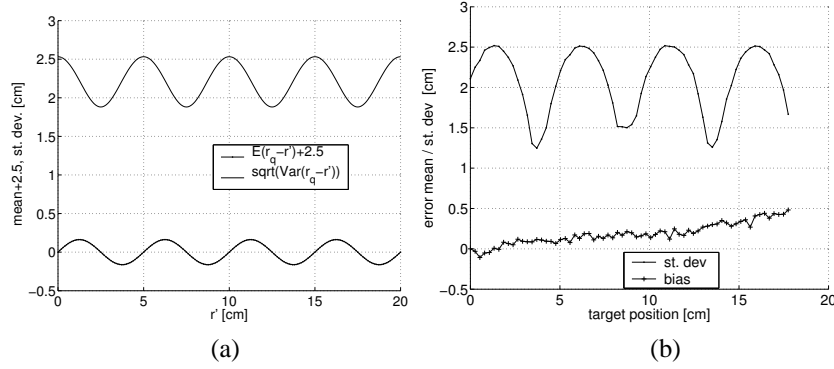
8

Figure 6: Effect of quantization on the PLS output: a) simulation, b) measurement

noise $r_n \sim N(0, \sigma_n^2)$ is added, and the result is fed into an ideal, truncating quantizer. Using the same approach as described in [2], the following equations were derived which describe the mean and variance of error in the truncating quantizer output if r' is given:

$$P(r_i|r') = F\left((i+1)\,q_r - r'; 0; \sigma_n^2\right) - F\left(iq_r - r'; 0; \sigma_n^2\right) \tag{17}$$

$$E(r_q - r') = \sum_{i=-\infty}^{+\infty} (iq_r - r')\, P(r_i|r') \tag{18}$$

$$var(r_q - r') = \left[\sum_{i=-\infty}^{+\infty} (iq_r - r')^2\, P(r_i|r')\right] - [E(r_q - r')]^2 \tag{19}$$

where $P(r_i|r')$ is the probability of the sensor returning range r_i given the true range r', F is the cumulative distribution function of a normal random variable, $q_r = 5\ cm$ is the quantization step and r_q is the output of the quantizer. When investigating the quantization effect in the output of the PLS sensor, Jensfelt in [8] presents similar equation as eq. (17,19), however he assumes a rounding quantizer, and doesn't consider the bias in the quantization error. A graph obtained by simulation of the change of the variance with the true distance is also shown in [8].

Figure 6a contains the results from eq. 17-19, for $\sigma_n = 1.7\ cm$. On the graph, the mean error was shifted up by half the quantization step (2.5 cm) for scaling reasons. The value of σ_n was chosen so that the noise standard deviation maximum of the quantizers output would match the measured one shown later. The knowledge of the noise standard deviation prior quantization (σ_n) is important for simulation purposes. From observing the simulation results, the mean error due to the quantizer, or quantization bias can be described as a sinusoid with a small amplitude:

$$r_{qb} = b \sin\left((r' - Q(r'))\frac{2\pi}{q_r}\right) - \frac{q_r}{2} \tag{20}$$

where $b = 0.16\ cm$ and $Q(r')$ is the quantized representation of r'. In theory, this quantization bias can generate a significant bias in the orientation of short measured lines. However, we will deal with this error later.

9

The standard deviation on fig. 6a can be described as

$$\sigma_r = k_1 \cos\left((r' - Q(r'))\frac{2\pi}{q_r}\right) + k_2 \tag{21}$$

where $k1 = 0.26\ cm$ and $k_2 = 2.25\ cm$.

Using our laser calibration tool, we measured the dependence of bias and standard deviation of the Sick PLS output on distance. In our experiment the laser calibration tools longitudinal axis was aligned with a laser beam. The target plane was moved by 20 cm further away from the laser in 2.5 mm steps. After each step, the plane stayed in position for 10 minutes to enable the collection of 3000 sample points. The PLS was used in 361 point mode, and the on board averaging of measurements was turned off. Because the precise distance of the Sick PLS and the laser calibration tool was unknown, the change of bias was being measured instead of the absolute value.

The result of the experiment is depicted on fig. 6b. The standard deviation is a periodic function with a period of the quantization step. In half of the period the standard deviation look like a sinusoid, which peaks at 2.5 cm. For the rest of the time it resembles a V shape.

The change in the bias, can be approximated with a linear function of distance with a slope of $0.5/18 \approx 0.03$. It is likely that just as in fig. 6a the bias has a periodic component, however it is hard to detect due to noise. It is unlikely that the rise of the bias was caused by a change in the temperature, since the PLS was allowed a 3 hour warm-up time prior the commencement of the experiment. Furthermore the range of a non moving point was also recorded during the experiment, and only about 1 mm drift was observed.

Our hypothetical explanation for the rise in the bias is the following: because the PLS uses laser as a light source, the illumination of the target surface doesn't depend on range (disregarding the divergence of the laser beam, and the attenuation of the air). However, if we assume a lambertian distribution of the reflected light, then the amount of reflected light reaching the photo receiver decreases with increasing range. Less light causes a slower rise time of the output signal of the photo receiver, which causes the object to appear further back. It is possible that the bias appears as linear only because the measurement interval was too short. We assume that the error gets reset by the compensation mechanism of the laser. The effect of the error on the precision of measured line parameters will be discussed later.

To find out the uncertainty of measured lines parameters due to random errors, we approximated the standard deviation of range measurements as constants, with the value of $\sigma_r = 2.4\ cm$. We did this for two reasons: firstly the variation in the standard deviation is not big compared to its mean (see fig. 6a). Secondly, if we take only one scan of a plane, we can not know which measurement has what standard deviation, therefore we assume the worst case.

We modeled the measurement covariance matrix as diagonal, because one range measurement is assumed to be uncorrelated with the value of other range measurements. Therefore we can use eq. 16 to determine the covariance of estimated line parameters. To show, that diagonal approximation of the measurement covariance matrix is not unrealistic, we have depicted on fig. 7 the covariance and correlation coefficient matrices for the first couple of points of lines 1 and 13 of figure 9. More details one the lines can be read in the next paragraph. The matrices can be viewed in their usual form in appendix B.1.

To justify our random error model, we conducted an experiment, where the robot was moving on an imaginary quarter circle of $R = 2$ m radius around our right angle
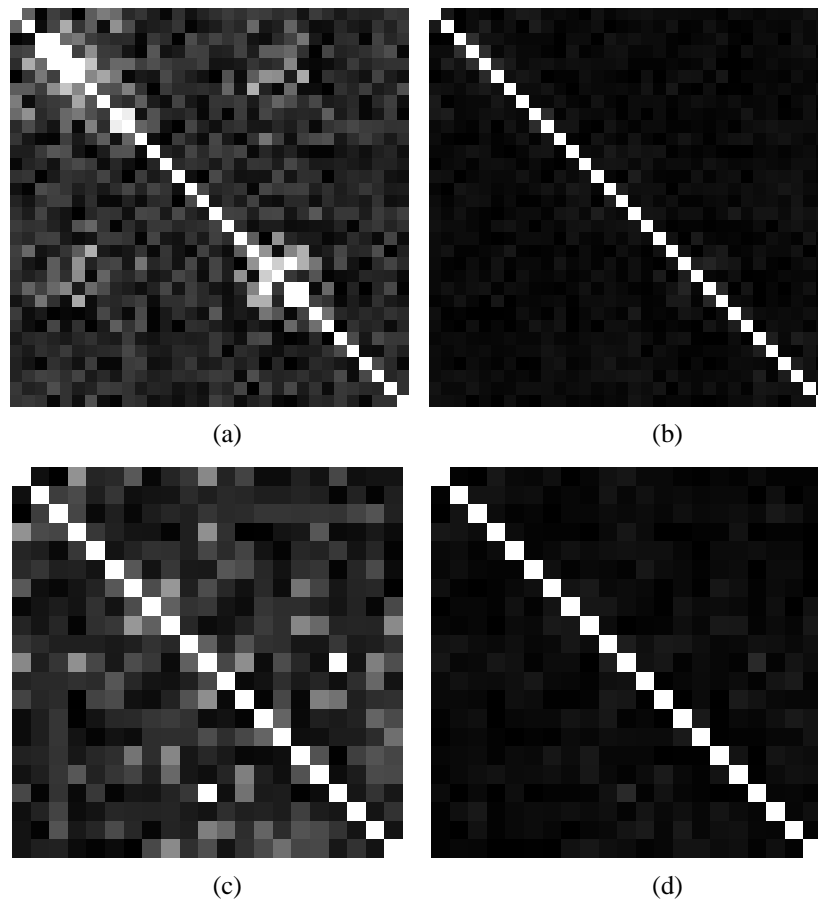
10

Figure 7: Covariance matrix a) and correlation coefficient matrix b) of the range readings for line 1, respectively for line 13 (c and d). Darker color means lower value.
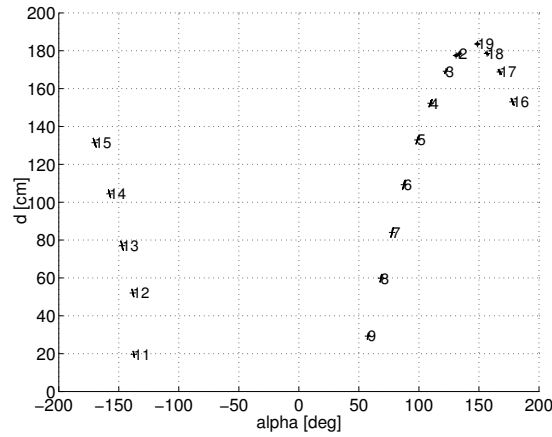
Figure 8: Parameters of lines taking part of the random noise model evaluation. $R = 2\,m$, $\Delta\theta = 10°$.

calibration tool. In each $\Delta\theta = 10°$ the robot stopped and turned toward the right angle to collect about 3000 scans. Using eq. 12-15 lines were fitted to the arms of the tool from each scan. Data from 20 lines were collected, whose parameters are depicted on fig. 8 in the line parameter space. Each line has also a number assigned to it for identification purposes. Then covariance for each set of line parameters was calculated using eq. 16. The results are shown on fig. 9, where the measured and estimated covariance matrices are represented as error ellipses. The probability of a point falling inside an ellipse is about 40%.

The previous experiment was repeated with the robot moving on a circle of R=1.5 m radius and stopping each $\Delta\theta = 5°$.

The error models are good enough most of the time, however in the case of line 1,2,19 of the first experiment, the measured covariances are slightly bigger than the predicted. The reason for this deviation is unknown. We suspect that our assumption of uncorrelated errors is violated since as it can be seen on fig. 9 the points of line 1,2 and 19 span through too few quantization levels. Therefore the information content of the measured points is smaller than modeled which results in optimistic covariance estimates. For lines 10, 20 the error ellipses are missing, because while being processed together, line 10 didn't have a sufficient number of points. On fig. 9 samples of points constituting the lines are shown.

The results of the second experiment (fig. 11 and fig. 12) are equally good as that of the first one except for those few cases where the measured line segment was pointing into the laser. For line number 18, the line was so well aligned with the laser, that only very few points represented the line segment, which resulted in a big difference between the measured and the predicted covariance matrix.

Remark

Figure fig. 10 and fig. 12 show error ellipses not just due to noisy laser output, but also due to errors in the extraction of the 2 arms of the right angle tool from the laser scans. Failing to identify the correct corner point in the data can lead to big errors especially, when one of the lines consists of only a few points. A presumably often used method

Figure 9: Raw data in Cartesian coordinate system to which lines were fitted. A "+" sign denotes the position of the laser. $R = 2\,m$, $\Delta\theta = 10°$.

Figure 10: Error ellipses of the measured (solid line) and estimated (dotted line) line parameter covariances plotted in line parameter space. Horizontal axis: angles, vertical axis: distances. $R = 2\,m,\ \Delta\theta = 10°$.
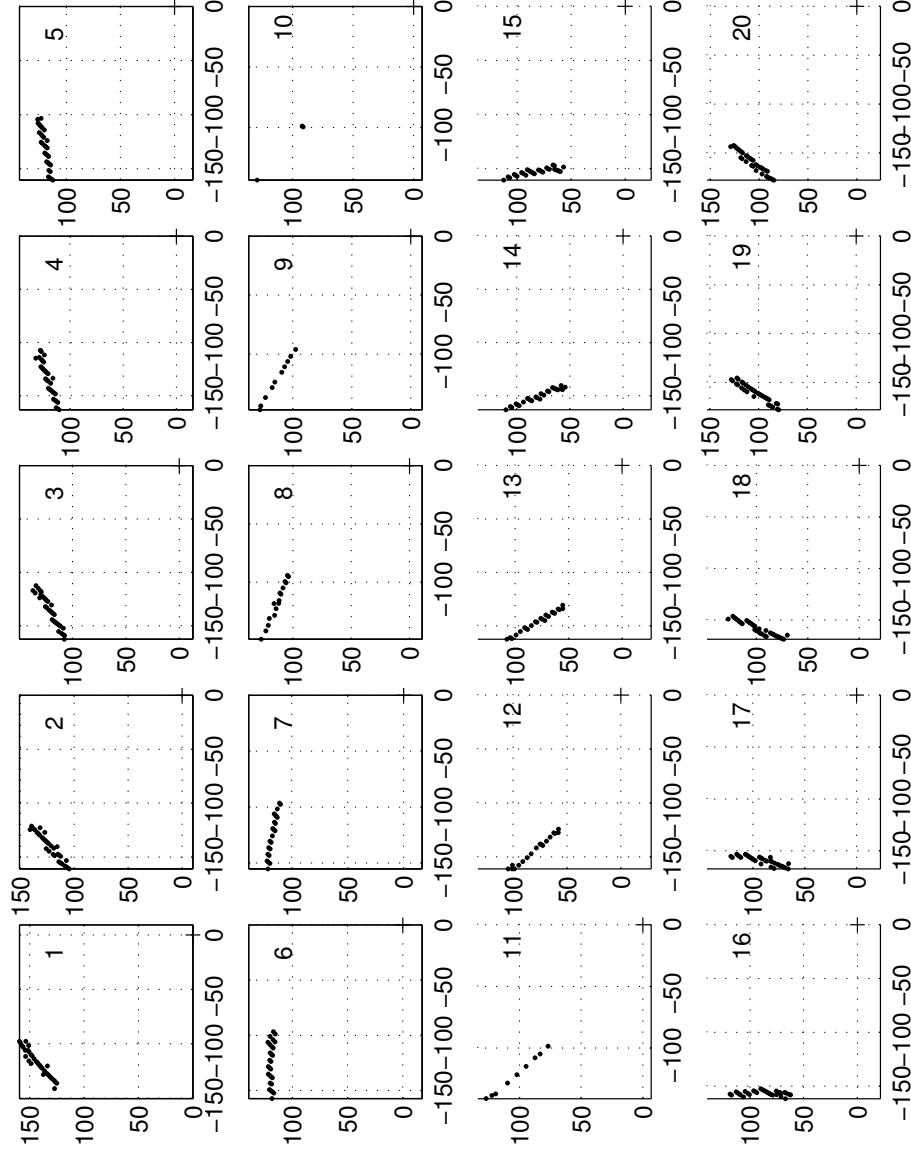
Figure 11: Raw data in Cartesian coordinate system to which lines were fitted. A "+" sign denotes the position of the laser. $R = 1.5 \, m$, $\Delta\theta = 5°$.
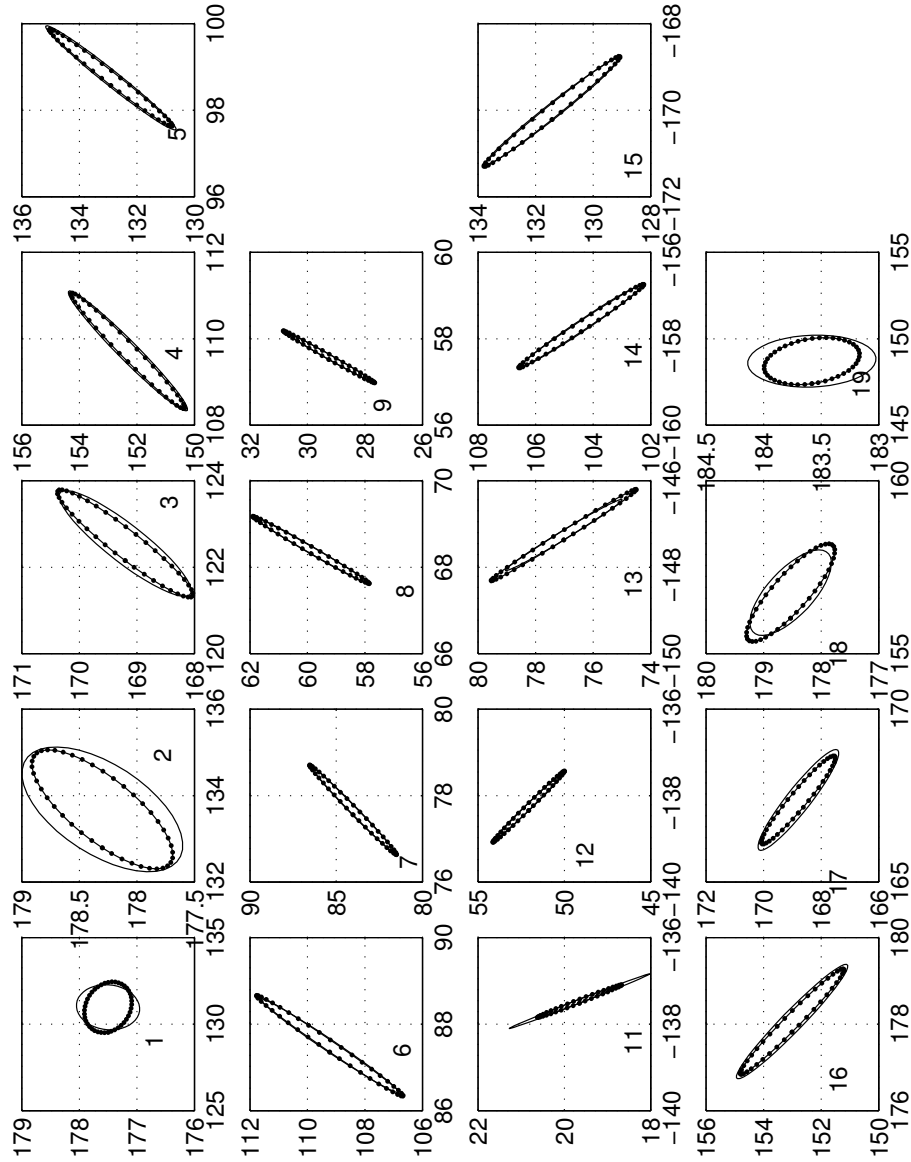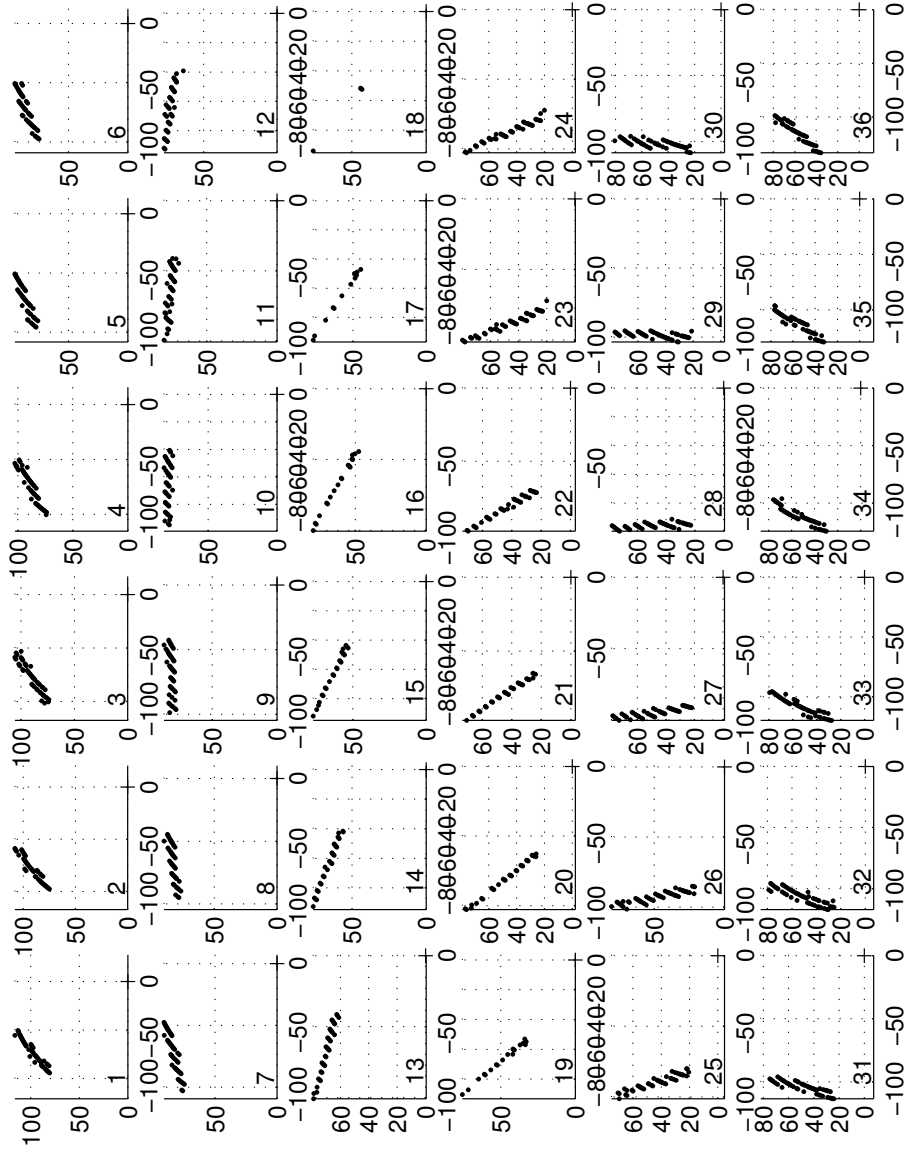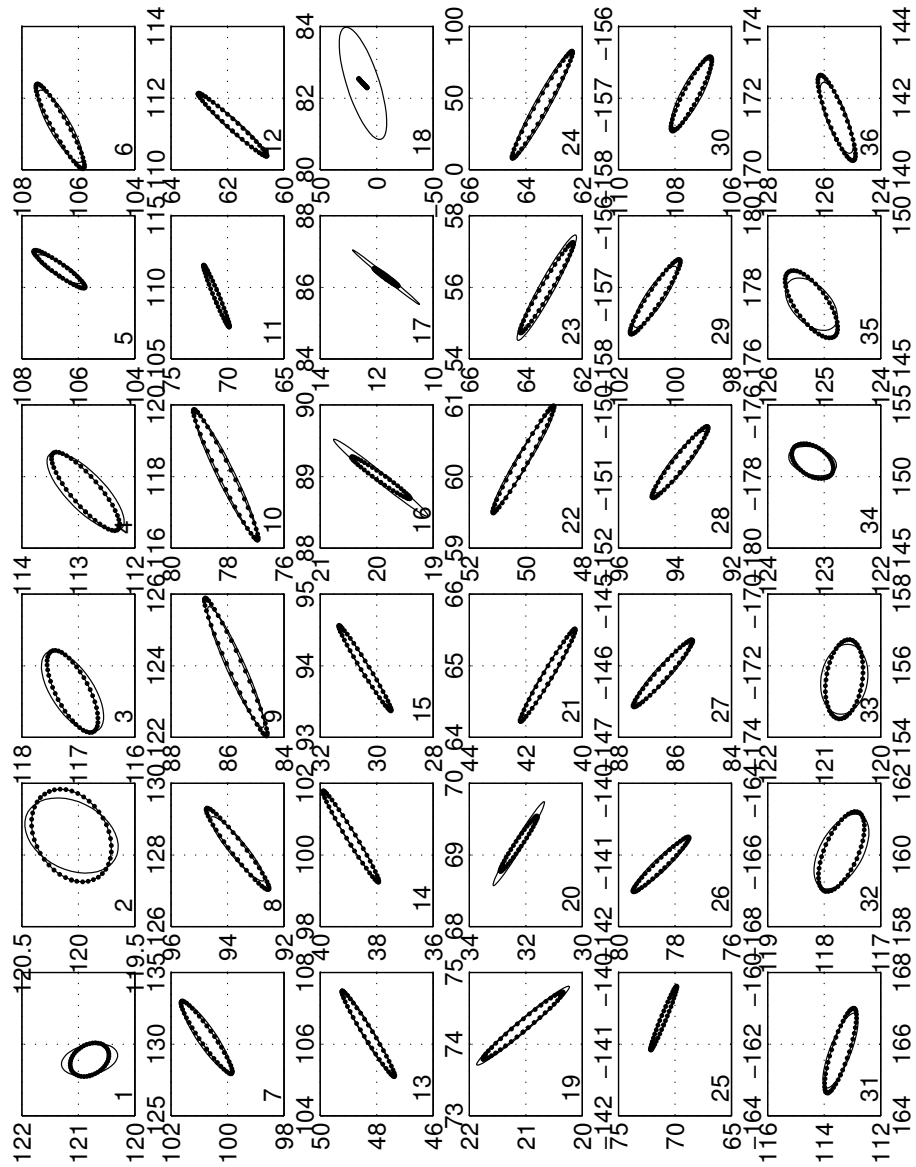
Figure 12: Error ellipses of the measured (solid line) and estimated (dotted line) line parameter covariances plotted in line parameter space. Horizontal axis: angles, vertical axis: distances. $R = 1.5\,m$, $\Delta\theta = 5°$.
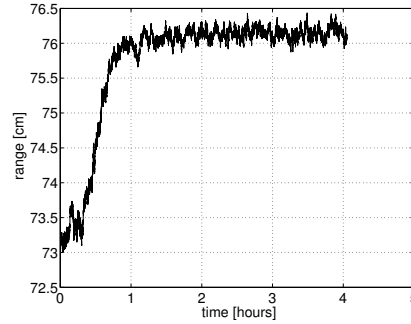
Figure 13: Change in filtered range readings during warm-up.

for corner point detection consists of finding the furthest point from a line defined by the two non-touching endpoints of the lines (see [5]). Due to the noisy nature of the laser output, this method often misses the right corner point. This problem can be solved by sacrificing some computing power. We have refined our choice of corner point by finding that point in the neighborhood of the initial corner point, which gives the minimum sum of error variances of both lines. Under error variance of a line we mean the variance of perpendicular distances of points from the line. The calculation of variances was performed by calculating the eigenvalues of the covariance matrix of the x and y coordinates of points, and choosing the smaller eigenvalue. Since the eigenvector of the largest eigenvalue points to the direction of the largest variance, therefore the eigenvalue associated with the other eigenvector which orthogonal to the first one represents the variance of points in the direction perpendicular to the line (see PCA).

2.5   Identical Bias in the Range Measurements

Bias of the same size in each range measurement of a scan appears as a curvature in a line which normally would look straight in a Cartesian coordinate system. Positive bias deforms lines to appear concave, and negative bias deforms lines to appear as convex.

As mentioned in subsection 2.4 there are instantaneous changes in bias of 1 cm amplitude in the range readings (see fig. 5). There can be different biases for different colors just as shown for LMS in [18]. Moreover bias in the range changes as the instrument heats up, just as reported in [18] for the SICK LMS sensor.

We have conducted a similar experiment to the one found in [18] with our PLS sensor, where we let the PLS measure a point on a wall for over 4 hours. We have observed a 3 cm drift in the readings (see fig. 13). In order to make the change in the measured range clearly visible, we filtered the raw readings with the following filter: $output(i) = 0.995output(i-1) + 0.005input(i)$, which is in our case equivalent to a first order linear filter with 40 s time constant. However, to be able to initialize the filter correctly, we applied the filter from the back to the front (eg. last value first, first value last).

In order to derive a formula which approximates the relation between bias in the range measurements and error in the angle and distance parameter of the measured line, we introduce the following assumptions:

17

- The measured line is horizontal, e.g. $\alpha = \frac{\pi}{2}$. We will show later, that this assumption has no effect on the result.

- If we do the analysis for a dataset containing no error except bias (r_b) in the range measurement, then the results will be valid for datasets containing random errors and quantized data as well.

If $\alpha = \pi/2$ then eq. 2 becomes

$$r = \frac{d}{\sin \phi} \tag{22}$$

and measured points in (X, Y) coordinate system become:

$$x_i = x_i' + x_{ei} = r_i' \cos \phi_i + r_b \cos \phi_i = d' \cot \phi_i + r_b \cos \phi_i \tag{23}$$

$$y_i = y_i' + y_{ei} = r_i' \sin \phi_i + r_b \sin \phi_i = d' + r_b \sin \phi_i \tag{24}$$

where x_i', y_i' are the true coordinates of a point on the line, x_{ei}, y_{ei} are errors due to bias, r_b is the bias in the range, d' is the true distance of the line from the origin (what we assume to know) and r_i' is the true range. In equation 23-24 r' was replaced by r from eq. 22.

The error in the slope k was calculated by substituting eq. 23-24 into 4:

$$k_e = k - k' = k - 0 =$$

$$= \frac{n \sum x_i' y_i' - \sum x_i' \sum y_i' + r_b d' \left(n \sum \cos \phi_i - \sum \cot \phi_i \sum \sin \phi_i\right) + r_b^2 \left(n \sum \cos \phi_i \sin \phi_i - \sum \cos \phi_i \sum \sin \phi_i\right)}{n \sum x_i'^2 - \left(\sum x_i'\right)^2 + 2 d' r_b \left(n \sum \frac{\cos^2 \phi_i}{\sin \phi_i} - \sum \cot \phi_i \sum \cos \phi_i\right) + r_b^2 \left(n \sum \cos^2 \phi_i - \left(\sum \cos \phi_i\right)^2\right)}$$

Because the line would be horizontal without bias, the sum of the terms containing x_i', y_i' in the nominator is 0. We found, that the coefficients at r_b^2 are much smaller that those at r_b, therefore they are neglected. After removing the small terms, k_e looks like:

$$k_e \approx \frac{d' r_b \left[n \sum \cos \phi_i - \sum \cot \phi_i \sum \sin \phi_i\right]}{n \sum x_i'^2 - \left(\sum x_i'\right)^2 + 2 d' r_b \left[n \sum \frac{\cos^2 \phi_i}{\sin \phi_i} - \sum \cot \phi_i \sum \cos \phi_i\right]} \tag{25}$$

To remove r_b from the denominator, we will linearize eq. 25 around $r_b = 0$ according to the following pattern:

$$ke = \frac{A r_b}{B + C r_b} \implies ke \approx \left[\frac{\partial}{\partial r_b} \frac{A r_b}{B + C r_b}\right]_{r_b=0} r_b =$$

$$= \left[\frac{AB}{(B + C r_b)^2}\right]_{r_b=0} r_b = \frac{AB}{B^2} r_b = \frac{A}{B} r_b \tag{26}$$

The result after the linearization is:

$$k_e \approx \frac{d' \left(n \sum \cos \phi_i - \sum \cot \phi_i \sum \sin \phi_i\right)}{n \sum x_i'^2 - \left(\sum x_i'\right)^2} r_b \tag{27}$$

Instead of x_i' it is possible to substitute:

$$x_i' = r_i' \cos \phi_i = \frac{d'}{\sin \phi_i} \cos \phi_i = d' \cot \phi_i \tag{28}$$

after that we get:

$$k_e \approx \frac{r_b}{d'} \frac{n \sum \cos \phi_i - \sum \cot \phi_i \sum \sin \phi_i}{n \sum \cot^2 \phi_i - \left(\sum \cot \phi_i\right)^2} \qquad (29)$$

At the derivation of the error in the y-intercept q_e, we used eq. 5 to get:

$$q_e = q - q' = \frac{1}{n} \left[\sum y_i - k_e \sum x_i\right] - \frac{1}{n} \left[\sum y_i' - k' \sum x_i'\right] \qquad (30)$$

Because our line is horizontal ($k' = 0$), therefore the term containing k' can be removed from eq. 30. Furthermore we have substituted eq. 23-24 into y_i and x_i to get:

$$q_e = \frac{1}{n} \left(\sum d' + r_b \sum \sin \phi_i - k_e \sum \left[d' \cot \phi_i + r_b \cos \phi_i\right] - \sum d'\right) =$$

$$= \frac{r_b}{n} \left(\sum \sin \phi_i - k_e \sum \cos \phi_i\right) - \frac{d' k_e}{n} \sum \cot \phi_i \qquad (31)$$

Our initial aim was to find out the error in the angle α_e and in the distance d_e. It is easy to show for $k_e \ll 1$, using a simplified version of eq. 6-7:

$$\alpha = \arccos \frac{-k}{\sqrt{1 + k^2}} \qquad (32)$$

$$d = \frac{q}{\sqrt{1 + k^2}} \qquad (33)$$

that $\alpha_e \approx k_e$ and $d_e \approx q_e$:

$$\alpha_e \approx \left[\frac{\partial}{\partial k} \arccos \frac{-k}{\sqrt{1 + k^2}}\right]_{k=0} k_e =$$

$$= \left[\frac{-1}{\sqrt{1 - \left(\frac{-k}{\sqrt{1+k^2}}\right)^2}} \left(-\frac{1}{\sqrt{1 + k^2}} + \frac{k^2}{\sqrt{(1 + k^2)^3}}\right)\right]_{k=0} k_e = k_e \qquad (34)$$

$$d_e \approx \left[\frac{\partial d}{\partial q}\right]_{\substack{k=0 \\ q=0}} q_e + \left[\frac{\partial d}{\partial k}\right]_{\substack{k=0 \\ q=0}} k_e =$$

$$= \left[\frac{1}{\sqrt{1 + k^2}}\right]_{\substack{k=0 \\ q=0}} q_e - \left[\frac{qk}{\sqrt{(1 + k^2)^3}}\right]_{\substack{k=0 \\ q=0}} k_e = q_e \qquad (35)$$

One might would want to treat r_b as a random variable because it probably changes with temperature, it also changes impulsively, and the exact value of r_b is unknown. Therefore we will show here how to derive a covariance estimate of the angle and distance error if r_b is a random variable with zero mean. For the sake of simplicity, lets introduce the following substitution:

$$k_e = A r_b \qquad (36)$$

$$q_e = B r_b - C r_b k_e - k_e D$$

$$= B r_b - A C r_b^2 - A D r_b \qquad (37)$$

where $A = \frac{1}{d} \frac{n \sum \cos \phi_i - \sum \cot \phi_i \sum \sin \phi_i}{n \sum \cot^2 \phi_i - (\sum \cot \phi_i)^2}$, $B = \frac{1}{n} \sum \sin \phi_i$, $C = \frac{1}{n} \sum \cos \phi_i$ and $D = \frac{1}{n} \sum \cot \phi_i$. Prior calculating the covariance matrix, we calculate the expectations for k_e and q_e:

$$\bar{k}_e = \mathrm{E}(k_e) = \mathrm{E}(Ar_b) = A\mathrm{E}(r_b) = A\bar{r}_b = 0 \tag{38}$$

$$\bar{q}_e = \mathrm{E}(q_e) = \mathrm{E}(Br_b - ACr_b^2 - ADr_b) =$$
$$= (B - AD)\mathrm{E}(r_b) - AC\mathrm{E}(r_b^2) = 0 - AC\sigma_{r_b}^2 \approx 0 \tag{39}$$

In eq. 39 we made a simplifying assumption of ACr_b^2 and therefore of $AC\sigma_{r_b}^2$ being so small that it can be approximated with 0. Then the elements of the covariance matrix were calculated as following:

$$\sigma_{k_e}^2 = \mathrm{E}(k_e^2) - (\mathrm{E}(k_e))^2 = \mathrm{E}(A^2 r_b^2) = A^2 \sigma_{r_b}^2 \tag{40}$$

$$\sigma_{q_e}^2 = \mathrm{E}(q_e^2) - (\mathrm{E}(q_e))^2 = \mathrm{E}((B - AD)^2 r_b^2) = (B - AD)^2 \sigma_{r_b}^2 \tag{41}$$

$$\sigma_{k_e q_e} = \mathrm{E}\left[(k_e - \bar{k}_e)(q_e - \bar{q}_e)\right] =$$
$$= \mathrm{E}(k_e q_e) = \mathrm{E}(Ar_b(B - AD)r_b) = A(B - AD)\sigma_{r_b}^2 \tag{42}$$

Then the resulting covariance matrix due to bias changing randomly will be:

$$C_b = cov(k_e, q_e) = cov(\alpha_e, d_e) = \begin{bmatrix} A^2 & (B - AD)A \\ (B - AD)A & (B - AD)^2 \end{bmatrix} \sigma_{r_b}^2 \tag{43}$$

At the beginning of this section, we have assumed that our line is horizontal. However, if we want to use eq. 29,31 and 43, all we have to do is to calculate A,B,C,D with angles normalized using:

$$\phi_i = \phi_{im} - \alpha + \frac{\pi}{2} \tag{44}$$

where α is the estimated angle of the line and ϕ_{im} are the measured bearings. Normalization has no effect on the error estimates $(\Delta\alpha, \Delta d)$, because this corresponds to a shift only in a polar coordinate system.

The computational burden at the calculation of the angle and distance error can be reduced if all sums in eq. (29, 31) are replaced with integrals, like:

$$\sum_{i=1}^{n} \sin \phi_i \approx \frac{n}{\Delta\phi} \int_{\phi_1}^{\phi_n} \sin \phi d\phi \tag{45}$$

where $\Delta\phi = \phi_n - \phi_1$. The error committed due to this approximation will be small due to the small angle resolution ($q_\phi = 0.5°$) of the laser. We substituted the following approximations:

$$\sum \cos \phi_i \approx \frac{n}{\Delta\phi} (\sin \phi_n - \sin \phi_1) \tag{46}$$

$$\sum \sin \phi_i \approx \frac{n}{\Delta\phi} (\cos \phi_1 - \cos \phi_n) \tag{47}$$

$$\sum \cot \phi_i \approx \frac{n}{\Delta\phi} (\ln |\phi_n| - \ln |\phi_1|) = \frac{n}{\Delta\phi} \ln \left| \frac{\sin \phi_n}{\sin \phi_1} \right| \tag{48}$$

$$\sum \cot^2 \phi_i \approx= \frac{n}{\Delta\phi} [\phi_1 + \cot \phi_1 - \phi_n - \cot \phi_n] = \frac{\cot \phi_1 - \cot \phi_n}{\Delta\phi} n - n \tag{49}$$
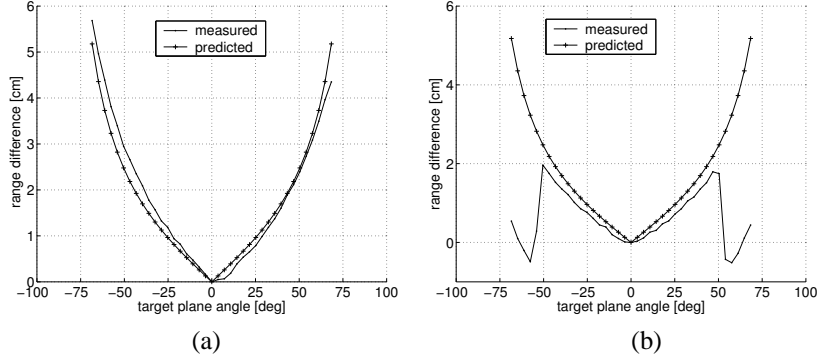
Figure 14: Measured range change depending on target plane angle

into eq. 29 and 31 to derive the following closed form solutions for the error in angle and distance:

$$\alpha_e \approx k_e = -\frac{r_b}{d'} \frac{\Delta\phi\left(\sin\phi_n - \sin\phi_1\right) + \ln\left|\frac{\sin\phi_n}{\sin\phi_1}\right|\left(\cos\phi_n - \cos\phi_1\right)}{\Delta\phi^2 + \Delta\phi\left(\cot\phi_n - \cot\phi_1\right) + \ln^2\left|\frac{\sin\phi_n}{\sin\phi_1}\right|} \qquad (50)$$

$$d_e \approx q_e = \frac{r_b}{\Delta\phi}\left(\cos\phi_1 - \cos\phi_n - k_e(\sin\phi_n - \sin\phi_1) - \frac{d'k_e}{r_b}\ln\left|\frac{\sin\phi_n}{\sin\phi_1}\right|\right) \qquad (51)$$

2.6   Error Changing with Incidence Angle

In paper [18] the authors measured the error in the range measurements of the LMS laser scanner. They found that the error in the range depends on the incidence angle of the beam and the plane. However, they provided no explanation for the source of this error, or any quantitative approximation of the error. We have conducted similar, but more elaborated experiments with our PLS. Our method for measuring the error change with incidence angle was the following:

We have aligned our laser calibration tool's longitudinal axis parallel with a line running on the floor. We have also made sure that the axis of rotation of the target plane was above the line. Then we have attempted to move our differential drive robot, so that the odometry center would be above the line. By observing the lasers output we tuned the robots position so that the target plane would appear as an odd number of points, with the center points having a bearing of $90°$. This way we could make sure, that there is a laser spot close to the center of rotation, and that the angle between our laser beam of interest and the target plane is about $90° \pm 2°$. In our next step we collected range readings, while moving the target plane from $0°$ (at this orientation the angle between plane and beam is $90°$) to $+50°$ and to $-50°$. If there was a difference between the average of range readings taken at $+50°$ and $-50°$ then we moved the laser calibration tool slightly to the left or right, depending on the sign of the difference. The amount of movement depended on the magnitude of the difference. We repeated this process iteratively until the ranges measured at $+50°$ and $-50°$ were equal.

After making sure that the center of our laser beam of interest coincides with the center of rotation, we started our experiment. In the experiments we have rotated the

21

target plane from $+70°$ to $-70°$ by $1.8°$ steps each 10 min. To avoid bias from quantization to influence our measurements, we repeated the measurements after moving the target plane away from the laser by half the quantization step, eg. by 2.5 cm. In the next step we computed the average range for each angle. To allow bias due to quantization to be cancelled, the average of the averages for the same angles, but different distances were calculated. Then from all the obtained results, the range value for $0°$ was subtracted.

Two examples of the results are shown in fig. 14, whereas the approximated ("predicted") error was calculated as $e_r = 2|\tan \beta|$, where β is the angle of the target plane. In fig. 14 a) the measured error is close to the approximated, however in fig. 14b it seems as if at angle $\pm 50°$, 2.5 cm was subtracted from the readings. A possible explanation for that is the following: as the target plane was rotated, less and less light came back to the laser scanner, causing longer and longer rise times of the output signal of the photo detector. We suspect, that at $\pm 50°$ the signal level got into a different band (see section 2.1), and the laser used different compensation values. In our experiments the jump in the range readings occurred at different angles for different laser to target plane distances. Also note that the $e_r = 2|\tan \beta|$ approximation was tested only with our target plane, which was coated with a non-glossy white paper, probably giving a good Lambertian reflection. It is possible that surfaces with more specularity would give different error characteristics.

2.6.1 Error Calculation

To approximate the bias in the estimated line parameters due to range errors changing with incidence angle, we would need to know where the range compensation jumps occur. Unfortunately, we don't have this information, therefore we will assume that by treating the errors as if there were no jumps (like fig. 14a), the results will represent the biggest possible error.

When estimating the bias error in the line parameter estimates, we first normalize the bearings of the line of interest:

$$\phi_i = \phi_{im} - \hat{\alpha} + \frac{\pi}{2} \tag{52}$$

to get a line parallel with the x axis. In eq. 52 $\hat{\alpha}$ is the estimated line angle and ϕ_{im} are the bearing of the laser range measurements. Then we calculate ranges which would have been measured by a perfect sensor of a line with the estimated parameters $(\hat{\alpha}, \hat{d})$:

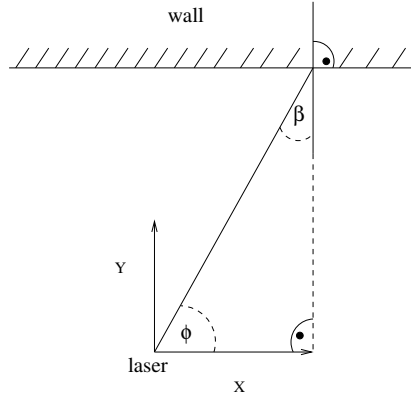$$r_i = \frac{\hat{d}}{\cos(\hat{\alpha} - \phi_{im})} = \frac{\hat{d}}{\sin(\phi_i)} \tag{53}$$

From experimental data (see fig. 14) the error for each range measurement is modelled as:

$$e_{ri} = w \left|\tan \beta_i\right| = w \left|\tan\left(\frac{\pi}{2} - \phi_i\right)\right| = w \left|\cot \phi_i\right| \tag{54}$$

where we exploited that for horizontal lines $\beta_i = \pi/2 - \phi_i$ (see fig. 15). In our case parameter w has a value of 2 cm. As the next step we convert our range measurements into (X, Y) coordinate system using:

$$x_i = (r_i + e_{ri}) \cos \phi_i \tag{55}$$

$$y_i = (r_i + e_{ri}) \sin \phi_i \tag{56}$$

22

Figure 15: The relation of ϕ and β for horizontal lines.

Finally all we have to do is to fit a line to (x_i, y_i) using linear regression (eq. 4-5), convert the resulting parameters into normal form (α, d) by the application of eq. 6-7, and calculate the errors as:

$$\Delta \alpha = \alpha - \frac{\pi}{2} \tag{57}$$

$$\Delta d = d - \hat{d} \tag{58}$$

For the derivation of a closed form solution, we have chosen a different approach.

2.6.2 Closed Form Error Calculation

Due the complexity of the problem, we shall linearize eq. 2 about the coordinates of the true line (α_0, d_0). Just as in subsection 2.5, we assume, that our true line is horizontal $(\alpha_0 = \pi/2)$. Therefore after substituting $\alpha_0 = \pi/2$ into eq. 8 we get:

$$\xi_i = r_i - r_{0i} \approx \frac{\Delta d}{\sin \phi_i} + \frac{d_0 \cos \phi_i}{\sin^2 \phi_i} \Delta \alpha = a_i \Delta d + b_i \Delta \alpha \tag{59}$$

where $a_i = \frac{1}{\sin \phi_i}$ and $b_i = \frac{d_0 \cos \phi_i}{\sin^2 \phi_i}$.

We can calculate $(\Delta \alpha, \Delta d)$ which minimizes the sum: $\sum \xi_i^2$, the following way (see appendix A.4):

$$\Delta \alpha = \frac{\sum \xi_{mi} a_i \sum a_i b_i - \sum \xi_{mi} b_i \sum a_i^2}{\left(\sum b_i a_i \right)^2 - \sum b_i^2 \sum a_i^2} \tag{60}$$

$$\Delta d = \frac{\sum \xi_{mi} b_i \sum a_i b_i - \sum \xi_{mi} a_i \sum b_i^2}{\left(\sum b_i a_i \right)^2 - \sum b_i^2 \sum a_i^2} \tag{61}$$

Where ξ_{mi} is the range error changing with the incidence angle, and it is calculated as:

$$\xi_{mi} = r_{mi} - r_{0i} = w|\tan \beta_i| = w|\tan \left(\frac{\pi}{2} - \phi_i \right)| = w|\cot \phi_i| = w s_i \cot \phi_i \tag{62}$$

Where $s_i = sign(\cot \phi_i)$.

If we substitute eq. 22 and 62 into eq. 60-61, we get:

$$numerator(\Delta \alpha) = \sum \xi_{mi} a_i \sum a_i b_i - \sum \xi_{mi} b_i \sum a_i^2 =$$

23

$$= \sum w s_i \cot \phi_i \frac{1}{\sin \phi_i} \sum d_0 \frac{\cos \phi_i}{\sin^3 \phi_i} - \sum w s_i \cot \phi_i d_0 \frac{\cos \phi_i}{\sin^2 \phi_i} \sum \frac{1}{\sin^2 \phi_i} =$$

$$= w d_0 \left(\sum s_i \frac{\cos \phi_i}{\sin^2 \phi_i} \sum \frac{\cos \phi_i}{\sin^3 \phi_i} - \sum s_i \frac{\cos^2 \phi_i}{\sin^3 \phi_i} \sum \frac{1}{\sin^2 \phi_i} \right) \quad (63)$$

$$denominator(\Delta \alpha, \Delta d) = d_0^2 \left[\left(\sum \frac{\cot \phi_i}{\sin^2 \phi_i} \right)^2 - \sum \frac{\cot^2 \phi_i}{\sin^2 \phi_i} \sum \frac{1}{\sin^2 \phi_i} \right] \quad (64)$$

$$numerator(\Delta d) = \sum \xi_{mi} b_i \sum a_i b_i - \sum \xi_{mi} a_i \sum b_i^2 =$$

$$= \sum w s_i \cot \phi_i d_0 \frac{\cos \phi_1}{\sin^2 \phi_i} \sum d_0 \frac{\cos \phi_i}{\sin^3 \phi_i} - \sum w s_i \cot \phi_i d_0 \frac{1}{\sin \phi_i} \sum d_0^2 \frac{\cos^2 \phi_i}{\sin^4 \phi_i}$$

$$= w d_0^2 \left(\sum s_i \frac{\cos^2 \phi_i}{\sin^3 \phi_i} \sum \frac{\cos \phi_i}{\sin^3 \phi_i} - \sum s_i \frac{\cos \phi_i}{\sin^2 \phi_i} \sum \frac{\cos^2 \phi_i}{\sin^4 \phi_i} \right) \quad (65)$$

To get a closed form solution, we use the following approximations, whereas the solutions for the integrals were taken from [7]:

$$\sum \frac{1}{\sin^2 \phi_i} \approx \frac{n}{\Delta \phi} \int_{\phi_1}^{\phi_n} \frac{1}{\sin^2 \phi_i} = \frac{n}{\Delta \phi} (- \cot \phi_n + \cot \phi_1) \quad (66)$$

$$\sum \frac{\cos \phi_i}{\sin^2 \phi_i} \approx \frac{n}{\Delta \phi} \int_{\phi_1}^{\phi_n} \frac{\cos \phi_i}{\sin^2 \phi_i} = \frac{n}{\Delta \phi} \left(-\frac{1}{\sin \phi_n} + \frac{1}{\sin \phi_1} \right) \quad (67)$$

$$\sum \frac{\cos \phi_i}{\sin^3 \phi_i} \approx \frac{n}{\Delta \phi} \int_{\phi_1}^{\phi_n} \frac{\cos \phi_i}{\sin^3 \phi_i} = \frac{n}{\Delta \phi} \left(-\frac{1}{2 \sin^2 \phi_n} + \frac{1}{2 \sin^2 \phi_1} \right) \quad (68)$$

$$\sum \frac{\cos^2 \phi_i}{\sin^4 \phi_i} \approx \frac{n}{\Delta \phi} \int_{\phi_1}^{\phi_n} \frac{\cos^2 \phi_i}{\sin^4 \phi_i} = \frac{n}{\Delta \phi} \left(-\frac{1}{3} \cot^3 \phi_n + \frac{1}{3} \cot^3 \phi_1 \right) \quad (69)$$

$$\sum \frac{\cos^2 \phi_i}{\sin^3 \phi_i} \approx \frac{n}{\Delta \phi} \int_{\phi_1}^{\phi_n} \frac{\cos^2 \phi_i}{\sin^3 \phi_i} =$$

$$= \frac{n}{\Delta \phi} \left(\frac{\cos \phi_1}{2 \sin^2 \phi_1} - \frac{\cos \phi_n}{2 \sin^2 \phi_n} + \frac{1}{2} \ln \left| \tan \frac{\phi_1}{2} \right| - \frac{1}{2} \ln \left| \tan \frac{\phi_n}{2} \right| \right) \quad (70)$$

However as we can see, s_i was left out from eq. 67,70. Because $s_i = |\cot \phi_i|$, $s_i = 1$ for $\phi \in (0, \pi/2)$ and $s_i = -1$ for $\phi \in (\pi/2, \pi)$. This means that in case of $\phi_1, \phi_n \leq \pi/2$ or $\phi_1, \phi_n \geq \pi/2$ we can move $s_i = s$ in front of the sums:

$$\sum s_i \frac{\cos^2 \phi_i}{\sin^3 \phi_i} \approx \frac{sn}{\Delta \phi} \left(\frac{\cos \phi_i}{2 \sin^2 \phi_i} + \frac{\cos \phi_n}{2 \sin^2 \phi_n} + \frac{1}{2} \ln \left| \tan \frac{\phi_1}{2} \tan \frac{\phi_n}{2} \right| \right) \quad (71)$$

$$\sum s_i \frac{\cos \phi_i}{\sin^2 \phi_i} \approx \frac{sn}{\Delta \phi} \left(\frac{1}{\sin \phi_1} - \frac{1}{\sin \phi_n} \right) \quad (72)$$

In case were $\phi_1 \leq \pi/2 \leq \phi_n$, the integrals in eq. 67,70 have to be broken down into two parts such as an integral from ϕ_1 to $\pi/2$ with $s_i = s = 1$ and an integral from $\pi/2$ to ϕ_n with $s_i = s = -1$:

$$\sum s_i \frac{\cos^2 \phi_i}{\sin^3 \phi_i} \approx= \frac{n}{\Delta \phi} \left[\int_{\phi_1}^{\frac{\pi}{2}} \frac{\cos^2 \phi}{\sin^3 \phi} d\phi - \int_{\frac{\pi}{2}}^{\phi_n} \frac{\cos^2 \phi}{\sin^3 \phi} d\phi \right] =$$

$$= \frac{n}{\Delta \phi} \left(\frac{\cos \phi_1}{2 \sin^2 \phi_1} + \frac{\cos \phi_n}{2 \sin^2 \phi_n} + \frac{1}{2} \ln \left| \tan \frac{\phi_1}{2} \tan \frac{\phi_n}{2} \right| \right) \quad (73)$$

24

$$\sum s_i \frac{\cos \phi_i}{\sin^2 \phi_i} \approx \frac{n}{\Delta\phi} \int_{\phi_1}^{\phi_n} \frac{\cos \phi_i}{\sin^2 \phi_i} d\phi =$$

$$= \frac{n}{\Delta\phi} \left[\int_{\phi_1}^{\frac{\pi}{2}} \frac{\cos \phi}{\sin^2 \phi} d\phi - \int_{\frac{\pi}{2}}^{\phi_n} \frac{\cos \phi}{\sin^2 \phi} d\phi \right] =$$

$$= \frac{n}{\Delta\phi} \left[-\frac{1}{\sin \frac{\pi}{2}} + \frac{1}{\sin \phi_1} + \frac{1}{\sin \phi_n} - \frac{1}{\sin \frac{\pi}{2}} \right] =$$

$$= \frac{n}{\Delta\phi} \left[-2 + \frac{1}{\sin \phi_1} + \frac{1}{\sin \phi_n} \right] \qquad (74)$$

Eq. 71 with eq. 73 and eq. 72 with eq. 74 can be merged together the following way:

$$\sum s_i \frac{\cos^2 \phi_i}{\sin^3 \phi_i} \approx \frac{ns}{\Delta\phi} F =$$

$$= \frac{ns}{\Delta\phi} \left(\frac{\cos \phi_1}{2\sin^2 \phi_1} + t\frac{\cos \phi_n}{2\sin^2 \phi_n} + \frac{1}{2} \ln \left| \tan \frac{\phi_1}{2} \right| + \frac{t}{2} \ln \left| \tan \frac{\phi_n}{2} \right| \right) \qquad (75)$$

$$\sum s_i \frac{\cos \phi_i}{\sin^2 \phi_i} \approx \frac{ns}{\Delta\phi} \left(-(t+1) + \frac{1}{\sin \phi_1} + \frac{t}{\sin \phi_n} \right) = \frac{nsE}{\Delta\phi} \qquad (76)$$

where

- $s = 1$, $t = 1$ for $\phi_1 \le \pi/2 \le \phi_n$.

- $s = 1$, $t = -1$ for $\phi_1, \phi_n \le \pi/2$.

- $s = -1$, $t = -1$ for $\phi_1, \phi_n \ge \pi/2$.

Thus the closed form solution for the line parameter error generated by range error changing with the incidence angle:

$$\Delta\alpha = \frac{ws}{d} \frac{EA - FC}{A^2 - \frac{1}{3}(\cot^3 \phi_1 - \cot^3 \phi_n)C} \qquad (77)$$

$$\Delta d = ws \frac{FA - ED}{A^2 - \frac{1}{3}(\cot^3 \phi_1 - \cot^3 \phi_n)C} \qquad (78)$$

where

$$A = \frac{1}{2} \left(\frac{1}{\sin^2 \phi_1} - \frac{1}{\sin^2 \phi_n} \right) \qquad (79)$$

$$C = \cot \phi_1 - \cot \phi_n \qquad (80)$$

$$D = \frac{1}{3} \left(\cot^3 \phi_1 - \cot^3 \phi_n \right) \qquad (81)$$

$$E = -(t+1) + \frac{1}{\sin \phi_1} + \frac{t}{\sin \phi_n} \qquad (82)$$

$$F = \frac{\cos \phi_1}{2\sin^2 \phi_1} + t\frac{\cos \phi_n}{2\sin^2 \phi_n} + \frac{1}{2} \ln | \tan \frac{\phi_1}{2}| + \frac{t}{2} \ln | \tan \frac{\phi_n}{2}| \qquad (83)$$

2.7 Error Due to Bias Growing with Distance

As it can be seen on fig. 6a, there is a bias in the range measurement, which grows with distance. However, we can assume, that this bias gets periodically reset by the PLS as

the signal amplitude on the output of the photo receiver gets into a different band (see sec. 2.1).

In our simplistic approximation of the error caused by this bias, we assumed, that the range error which is added to the true ranges grows linearly from 0 for the shortest range, up to the maximum value (but no more than max_err) for the longest range. The rate of growth is either $v_r = 0.5/18 \approx 0.03$ or a smaller number which results in a maximum error of max_err. We followed the same path in the calculations as in 2.6.1, except for the calculation of e_{ri} which was performed in the following way:

$$r_{max} = max(r)$$
$$r_{min} = min(r)$$
$$\Delta r = min((r_{max} - r_{min})v_r, max\_err)$$
$$r_{ei} = (r_i - r_{min})\frac{\Delta r}{r_{max} - r_{min}} = (r_i - r_{min})k \tag{84}$$

For the choice of max_err values between 5 and 13 seem to be reasonable.

To get formulas, which can be possibly converted into a closed form solution, eq. 22 was substituted into eq. 84 and the result was substituted into eq. 60-61:

$$numerator(\Delta\alpha) = \sum \xi_{mi}a_i \sum a_ib_i - \sum \xi_{mi}b_i \sum a_i^2 =$$
$$= \sum r_{ei}\frac{1}{\sin\phi_i} \sum d_0\frac{\cos\phi_i}{\sin^3\phi_i} - \sum r_{ei}d_0\frac{\cos\phi_i}{\sin^2\phi_i} \sum \frac{1}{\sin^2\phi_i} =$$
$$= \sum d_0 k\left(\frac{1}{\sin(\phi_i)} - \frac{1}{\sin\phi_{min}}\right)\frac{1}{\sin\phi_i} \sum d_0\frac{\cos\phi_i}{\sin^3\phi_i} -$$
$$- \sum d_0 k\left(\frac{1}{\sin(\phi_i)} - \frac{1}{\sin\phi_{min}}\right)d_0\frac{\cos\phi_i}{\sin^2\phi_i} \sum \frac{1}{\sin^2\phi_i} =$$
$$= \frac{d_0^2 k}{\sin\phi_{min}}\left(\sum \frac{1}{\sin^2\phi} \sum \frac{\cos\phi_i}{\sin^2\phi_i} - \sum \frac{1}{\sin\phi} \sum \frac{\cos\phi_i}{\sin^3\phi_i}\right) \tag{85}$$

$$numerator(\Delta d) = \sum \xi_{mi}b_i \sum a_ib_i - \sum \xi_{mi}a_i \sum b_i^2 =$$
$$= \sum r_{ei}\frac{d_0\cos\phi_i}{\sin^2\phi_i} \sum d_0\frac{\cos\phi_i}{\sin^3\phi_i} - \sum r_{ei}\frac{1}{\sin\phi_i} \sum \frac{d_0^2\cos^2\phi_i}{\sin^4\phi_i} =$$
$$= d_0^3 k\left(\sum \left(\frac{1}{\sin(\phi_i)} - \frac{1}{\sin\phi_{min}}\right)\frac{\cos\phi_i}{\sin^2\phi_i} \sum \frac{\cos\phi_i}{\sin^3\phi_i}\right) -$$
$$- d_0^3 k\left(\sum \left(\frac{1}{\sin(\phi_i)} - \frac{1}{\sin\phi_{min}}\right)\frac{1}{\sin\phi_i} \sum \frac{\cos^2\phi_i}{\sin^4\phi_i}\right)$$
$$= d_0^3 k\left(\sum \frac{\cos\phi_i}{\sin^3\phi_i} - \frac{1}{\sin\phi_{min}} \sum \frac{\cos\phi_i}{\sin^2\phi_i}\right) \sum \frac{\cos\phi_i}{\sin^3\phi_i}$$
$$- d_0^3 k\left(\sum \frac{1}{\sin^2\phi_i} - \frac{1}{\sin\phi_{min}} \sum \frac{1}{\sin\phi_i}\right) \sum \frac{\cos^2\phi_i}{\sin^4\phi_i} \tag{86}$$

$$denominator(\Delta\alpha, \Delta d) = d_0^2 \left[\left(\sum \frac{\cot\phi_i}{\sin^2\phi_i}\right)^2 - \sum \frac{\cot^2\phi_i}{\sin^2\phi_i} \sum \frac{1}{\sin^2\phi_i}\right] \tag{87}$$

Then we used the following approximations, whereas the solutions for the integrals were taken from [7]:

$$\sum \frac{1}{\sin\phi_i} \approx \frac{n}{\Delta\phi}\int_{\phi_1}^{\phi_n} \frac{1}{\sin\phi_i} = \frac{n}{\Delta\phi}\ln\left|\frac{\tan\frac{\phi_n}{2}}{\tan\frac{\phi_1}{2}}\right| \tag{88}$$

$$\sum \frac{1}{\sin^2 \phi_i} \approx \frac{n}{\Delta\phi} \int_{\phi_1}^{\phi_n} \frac{1}{\sin^2 \phi_i} = \frac{n}{\Delta\phi}(-\cot \phi_n + \cot \phi_1) \tag{89}$$

$$\sum \frac{\cos \phi_i}{\sin^2 \phi_i} \approx \frac{n}{\Delta\phi} \int_{\phi_1}^{\phi_n} \frac{\cos \phi_i}{\sin^2 \phi_i} = \frac{n}{\Delta\phi}\left(-\frac{1}{\sin \phi_n} + \frac{1}{\sin \phi_1}\right) \tag{90}$$

$$\sum \frac{\cos \phi_i}{\sin^3 \phi_i} \approx \frac{n}{\Delta\phi} \int_{\phi_1}^{\phi_n} \frac{\cos \phi_i}{\sin^3 \phi_i} = \frac{n}{\Delta\phi}\left(-\frac{1}{2\sin^2 \phi_n} + \frac{1}{2\sin^2 \phi_1}\right) \tag{91}$$

$$\sum \frac{\cos^2 \phi_i}{\sin^4 \phi_i} \approx \frac{n}{\Delta\phi} \int_{\phi_1}^{\phi_n} \frac{\cos^2 \phi_i}{\sin^4 \phi_i} = \frac{n}{\Delta\phi}\left(-\frac{1}{3}\cot^3 \phi_n + \frac{1}{3}\cot^3 \phi_1\right) \tag{92}$$

$$\tag{93}$$

The resulting closed form solutions are:

$$\Delta\alpha = \frac{k}{\sin \phi_{min}} \frac{B(\cot \phi_1 - \cot \phi_n) - A\ln\left|\frac{\tan \frac{\phi_n}{2}}{\tan \frac{\phi_1}{2}}\right|}{A^2 - \frac{1}{3}\left(\cot^3 \phi_1 - \cot^3 \phi_n\right)\left(\cot \phi_1 - \cot \phi_n\right)} \tag{94}$$

$$\Delta d = d_0 k \frac{A\left(A - \frac{B}{\sin \phi_{min}}\right) - \frac{1}{3}\left[\cot \phi_1 - \cot \phi_n - \frac{\ln\left|\frac{\tan \frac{\phi_n}{2}}{\tan \frac{\phi_1}{2}}\right|}{\sin \phi_{min}}\right]\left(\cot^3 \phi_1 - \cot^3 \phi_n\right)}{A^2 - \frac{1}{3}\left(\cot^3 \phi_1 - \cot^3 \phi_n\right)\left(\cot \phi_1 - \cot \phi_n\right)} \tag{95}$$

where ϕ_{min} is the bearing corresponding to r_{min} and

$$A = \frac{1}{2\sin^2 \phi_1} - \frac{1}{2\sin^2 \phi_n} \tag{96}$$

$$B = \frac{1}{\sin \phi_1} - \frac{1}{\sin \phi_n} \tag{97}$$

2.8 Error Due to Quantization Bias

As it was shown in sec. 2.4 using simulations, the truncating quantizer introduces a bias which can be described by:

$$r_{qb} = b\sin((r' - Q(r'))\frac{2\pi}{q_r}) - \frac{q_r}{2} \tag{98}$$

This quantization bias superimposed on the true range can cause a systematic error in the estimated line parameters. Unfortunately the true range r' is unknown, therefore the precise calculation of the angle and distance error of a line is probably not possible. However, it is possible to find a rough approximate for the maximum error. Lets assume the following:

- The $\frac{q_r}{2}$ error term in eq. 98 is taken care of by the manufacturer, or its contribution to the overall error is modeled as constant bias (see sec. 2.5).

- Our line parameters are reasonably accurate, therefore our estimate of r' differs from r' only by a constant, which causes a phase shift in the range bias.

- The line in question is normalized.

Then we can approximate the maximum errors by varying the superimposed sinusoids phase and finding the maximum error. Note that by varying the phase of the sinusoid,

the nonlinearity in eq. 98 represented by the quantizer $Q(r')$ doesn't stop us from deploying standard analysis tools to find the maximum error.

Lets rewrite eq. 98 so that it contains a phase shift ϵ:

$$r_{qb} = b\sin\left((r' - Q(r'))\frac{2\pi}{q_r}\right) \approx b\sin\left((r - Q(r))\frac{2\pi}{q_r} + \epsilon\right) = b\sin(\delta + \epsilon) \quad (99)$$

where r is calculated using the estimated line parameters.
To find out the error in orientation caused by the quantization bias, r_{qb} of eq. 99 is substituted into ξ_{mi} of eq. 60:

$$\Delta\alpha = \frac{\sum \xi_{mi} a_i \sum a_i b_i - \sum \xi_{mi} b_i \sum a_i^2}{\left(\sum b_i a_i\right)^2 - \sum b_i^2 \sum a_i^2} = \quad (100)$$

$$= \frac{1}{M}\left(\sum r_{qbi} a_i \sum a_i b_i - \sum r_{qbi} b_i \sum a_i^2\right) = \quad (101)$$

$$= \frac{1}{M}\left(\sum r_{qbi} a_i C_1 - \sum r_{qbi} b_i C_2\right) = \quad (102)$$

$$= \frac{b}{M}\left(C_1 \sum \sin(\delta_i + \epsilon)a_i - C_2 \sum \sin(\delta_i + \epsilon)b_i\right) \quad (103)$$

To find out where $\Delta\alpha$ peaks we differentiate $\Delta\alpha$ by ϵ and find where does it equal to zero:

$$\frac{\partial\Delta\alpha}{\partial\epsilon} = \frac{b}{M}\left(C_1 \sum \cos(\delta_i + \epsilon)a_i - C_2 \sum \cos(\delta_i + \epsilon)b_i\right) = 0 \quad (104)$$

Under the conditions that $b \neq 0$ and $M \nrightarrow \infty$, eq. 104 is equivalent to

$$0 = C_1 \sum \cos(\delta_i + \epsilon)a_i - C_2 \sum \cos(\delta_i + \epsilon)b_i =$$
$$= \cos\epsilon\left(C_1 \sum a_i \cos\delta_i - C_2 \sum b_i \cos\delta_i\right) -$$
$$- \sin\epsilon\left(C_1 \sum a_i \sin\delta_i - C_2 \sum b_i \sin\delta_i\right) = 0 \quad (105)$$

From eq. 105, ϵ corresponding to an extreme of $\Delta\alpha$ can be found as:

$$\epsilon_{m\alpha} = \arctan\frac{C_1 \sum a_i \cos\delta_i - C_2 \sum b_i \cos\delta_i}{C_1 \sum a_i \sin\delta_i - C_2 \sum b_i \sin\delta_i} \quad (106)$$

To find an extreme of Δd, the above mentioned process has to be repeated, with the difference that eq. 61 has to be differentiated with respect to ϵ.

Δd is expressed as:

$$\Delta d = \frac{\sum r_{qbi} b_i \sum a_i b_i - \sum r_{qbi} a_i \sum b_i^2}{\left(\sum b_i a_i\right)^2 - \sum b_i^2 \sum a_i^2} =$$
$$= \frac{\sum r_{qbi} b_i C_1 - \sum r_{qbi} a_i C_3}{M} \quad (107)$$

To make the differentiation of Δd easier, we first differentiate r_{qbi}:

$$\frac{\partial r_{qbi}}{\partial\epsilon} = b\cos(\delta_i + \epsilon) = b\left(\cos\delta_i \cos\epsilon - \sin\delta_i \sin\epsilon\right) \quad (108)$$

28

The differential of Δd is the combination of eq. 107 and 108:

$$\frac{\partial \Delta d}{\partial \epsilon} = \frac{b}{M} C_1 \sum \left(\cos \delta_i \cos \epsilon - \sin \delta_i \sin \epsilon \right) b_i -$$
$$\frac{b}{M} C_3 \sum \left(\cos \delta_i \cos \epsilon - \sin \delta_i \sin \epsilon \right) a_i \tag{109}$$

The maximum distance error can be obtained by solving $\frac{\partial \Delta d}{\partial \epsilon} = 0$, which is equivalent to:

$$\cos \epsilon \left(C_1 \sum b_i \cos \delta_i - C_3 \sum a_i \cos \delta_i \right) -$$
$$- \sin \epsilon \left(C_1 \sum b_i \sin \delta_i - C_3 \sum a_i \sin \delta_i \right) = 0 \tag{110}$$

From where ϵ generating the maximal distance error:

$$\epsilon_{md} = \arctan \frac{C_1 \sum b_i \cos \delta_i - C_3 \sum a_i \cos \delta_i}{C_1 \sum b_i \sin \delta_i - C_3 \sum a_i \sin \delta_i} \tag{111}$$

where

$$C_1 = \sum a_i b_i, \;\; C_2 = \sum a_i^2, \;\; C_3 = \sum b_i^2, \;\; \delta_i = (r_i - Q(r_i)) \frac{2\pi}{q_r} \tag{112}$$

2.9 Error Due to Laser Plane Misalignment

The robot which has our PLS laser scanner is mounted on it, is equipped with two pneumatic tires and two caster wheels, one of which is suspended on springs. The laser plane orientation depends on the tire pressures and on the orientation of the caster wheels. We found that the laser plane pitch angle changes by $0.4°$ just by moving the caster wheels around. We also found one time that the roll angle was $1°$, due to not equal tire pressures.

In our analysis of the error due to laser plane misalignment, homogenous transformations (see for example [12]) were used in 3D space. Lets place a world coordinate system (denoted with subscript "w") into the center of the odometry of the robot with the (X,Y) plane parallel with the floor, and Y axis pointing toward the front of the robot. Lets place a second, robot coordinate system denoted with subscript "r", into the center of odometry. We get this new coordinate system by rotating the world coordinate system around its X axis by the pitch angle β, and then rotating the result around its new Y axis by the roll angle γ. Lets place a new coordinate system for the laser, denoted by "l", which has the same orientation as the robot coord. syst. but it is displaced by the coordinates of the laser $(x_l, y_l, z_L, 1)^t$. Then to find out how a point measured in the misaligned laser coordinate system would appear in a well aligned laser coordinate system, we have to multiply the homogeneous coordinates of the measured point with a transformation matrix which is the product of 4 homogeneous transform matrices:

$$v_{wl} = T^{-1} R_x(\beta) R_y(\gamma) T v_{rl} =$$

$$= \begin{bmatrix} 1 & 0 & 0 & x_l \\ 0 & 1 & 0 & y_l \\ 0 & 0 & 1 & z_l \\ 0 & 0 & 0 & 1 \end{bmatrix}^{-1} \begin{bmatrix} 1 & 0 & 0 & 0 \\ 0 & cos\beta & -sin\beta & 0 \\ 0 & sin\beta & cos\beta & 0 \\ 0 & 0 & 0 & 1 \end{bmatrix}.$$

$$\cdot \begin{bmatrix} cos\gamma & 0 & -sin\gamma & 0 \\ 0 & 1 & 0 & 0 \\ sin\gamma & 0 & cos\gamma & 0 \\ 0 & 0 & 0 & 1 \end{bmatrix} \begin{bmatrix} 1 & 0 & 0 & x_l \\ 0 & 1 & 0 & y_l \\ 0 & 0 & 1 & z_l \\ 0 & 0 & 0 & 1 \end{bmatrix} \begin{bmatrix} x_r \\ y_r \\ z_r \\ 1 \end{bmatrix}$$

Now lets assume that the (X,Y) axes of the laser are aligned with the (X,Y) axes of the robot coordinate system. Note, that in this configuration the laser is pointing forward. Lets assume that all walls are perpendicular to the floor. Then an equation of a plane representing a wall is given by the equation:

$$\omega_{rl}^T v_{rl} = \begin{bmatrix} \cos\alpha & \sin\alpha & 0 & -d \end{bmatrix} v_{rl} = 0 \tag{113}$$

To find out the difference in the perception of a plane in case of a non zero roll/pitch angle, we transform the plane parameters (see [12]) expressed in the laser coordinate system on the robot to the laser coordinate system in the world coordinate system, which represents the ideal case with zero roll and pitch angles:

$$\omega_{wl} = (T^{-1}R_x(\beta)R_y(\gamma)T)^T \omega_{rl} \tag{114}$$

To extract the line from the result, we need to calculate the intersection of ω_{wl} with the (X,Y) plane, after which we get the equation for the line as:

$$x\cos\gamma\cos\alpha + y(\cos\beta\sin\alpha - \sin\gamma\sin\beta\cos\alpha) =$$
$$= d - (x_l\cos\gamma - y_l\sin\gamma\sin\beta - z_l\sin\gamma\cos\beta - x_l)\cos\alpha -$$
$$- (y_l\cos\beta - z_l\sin\beta - y_l)\sin\alpha \tag{115}$$

The representation of a line in eq. 115 is not in normal form, because the coefficients at x and y are not normalized. Lets denote the coefficient at x as c_x the coefficient at y as c_y and the right side as c_d. Then our line in slope-intercept form:

$$y = -\frac{c_x}{c_y}x + \frac{c_d}{c_y} = kx + q \tag{116}$$

At last (k,q) can be converted into (α', d') using eq. 6-7. The a difference between α' and α and between d' and d gives the error in the angle and distance parameters of a line when the laser plane is not parallel with the floor.

After experimenting with parameters of lines, roll,pitch angles and laser positions, we observed that the effect of laser plane misalignment on the line parameters is insignificant if the roll and pitch angles are reasonably small, and the laser is placed close to the center of odometry. To show an example, lets assume that the laser is placed at $(0, 30cm)$ in the robots coordinate system, and that the wall to be measured can be described by $\alpha = 90°$ and $d = 200$ cm. This configuration would lead to the following errors:

- $\beta = \gamma = 1° \implies \Delta\alpha = -0.0175°, \; \Delta d = 0.0194cm.$

- $\beta = \gamma = 3° \implies \Delta\alpha = -0.1572°, \; \Delta d = 0.1745cm.$

- $\beta = \gamma = 5° \implies \Delta\alpha = -0.4369°, \; \Delta d = 0.4827cm.$

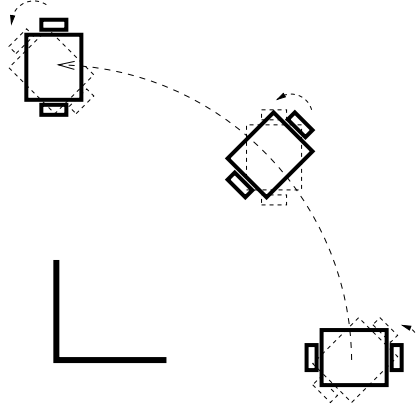- $\beta = \gamma = 10° \implies \Delta\alpha = -1.7538°, \; \Delta d = 1.8924cm.$

Figure 16: Robot moving around a perfect corner in our systematic error test.

3 Experimental Testing of the Systematic Error Model

We have performed only indirect tests of the angle systematic error estimate because precise testing of estimated line parameter precision is quite complicated and/or time consuming. In our experiments we were using our "perfect" corner tool, whose opening angle we estimated as $89.85° \pm 0.3°$. In our experiments our robot was moving on a path resembling an arc around our "perfect" corner tool as can be seen on fig. 16. On its course the robot stopped each few degrees, turned toward the corner and took thousands of scans.

Lines were fitted to the arms of the tool in the scans, and the average angle difference was evaluated for each position. On position we mean the ordinal number of the place where the robot stopped and turned towards the corner to collect scans. We assumed that the averages were influenced only by systematic errors, because each average was calculated from about 3000 samples. The opening angle of the corner was estimated by calculating the difference of the estimated angles of the corner arms.

When approximating the systematic error in angle estimates, errors due to identical bias, errors changing with incidence angle, errors due to bias growing with distance and errors due to quantization bias were considered only. Errors due to laser plane misalignment were neglected. The systematic error estimates were calculated only for the first scan taken at each position. In the error calculation, the average angle and distance parameters were used. The absolute values of the errors from all 4 error sources for both lines were summed up to create a worst case estimate.

The following parameters were used at the systematic error calculations:

- Identical bias parameter: $\sigma_{rb} = 5\ cm$.

- Incidence angle error parameter: $w = 2$.

- Error growing with distance parameter: $v_r = 0.03,\ max\_err = 13\ cm$.

- Quantization bias parameter: $b = 0.17\ cm$.

There were 3 experiments conducted. In the first experiment, the robot was moving on an arc of radius $R = 1.5\ m$ around the "perfect" corner, and stopped to collect scans

31

at each $\Theta = 5°$. A sample scan taken at each position is shown on fig. 17. Each sub-figure of fig. 17 is numbered the same way as the resulting opening angles on fig. 18. On fig. 18 the estimated error bounds are marked with a "*" and a "+".

In the second experiment the robot moved on an arc of $R = 2\ m$ radius and took scans each $\Theta = 10°$. The results can be seen on fig. 19-20.

In the third experiment the robot moved on an arc of $R = 3\ m$ radius and took scans each $\Theta = 5°$. The results can be seen on fig. 21-22.

From fig. 18,20, 22 we can see that the measured systematic error reached $4°$ in several cases. It would be good to know if in such cases the systematic or the non-systematic error is larger. Luckily our first experiments dataset was reused in sec. 2.4 at the random error experiment. Therefore if we want to know how big were the random errors at position 9 of experiment 1 (the systematic error is almost $4°$, see fig. 18), then all we need to do is to look at sub-figure 9 and 9+18=27 of figure 12. From there we can see, that the angle standard deviation of both arms is about $1°$. Therefore we can conclude that systematic errors in estimated line parameters can be bigger than the random ones!

When evaluating our random error models, we need to know that if we would have a perfect systematic error model, then either the upper, or the lower error mark would lie on the $-90°$ mark of fig. 18,20, and 22. However as we see, the errors are most of the time bigger. This is normal, because we added up the absolute values of angle errors from each error source, thus creating a worst case estimate. In reality, these errors some times cancel out each other.

In our models we didn't consider the compensation mechanism of the laser either, which corrects readings by measuring the peak of a returned signal. The reason is that we don't have access to any of the internal parameters including the measured signal strength. Compensation can reduce the line parameter errors, or it can increase them depending on where it happens.

In some instances our estimated error was smaller than the measured one. It is more than likely than there are other error sources involved which were not modeled. One such error source is the error caused by wrong segmentation of the arms of the right angle calibration tool. Because range measurements are noisy, the determination of where one arm ends and the second arm starts is hard. Errors in the segmentation can cause systematic errors in some line parameters because points associated with the wrong arm can lie in some cased always on one side of the arm.

4 Conclusion and Future Work

In this tech report, the results of our investigations of line segment parameter estimation from laser range data are summarized. All observations are based upon only one particular Sick PLS 101-112 laser range finder. An approach for line parameter estimation was developed in which parameters of a line are estimated directly in the lasers polar coordinate system, without the conversion of measurements into a Cartesian coordinate system (except for getting an initial estimate). This line parameter estimation method allows a satisfactory line parameter uncertainty estimation, which has been verified experimentally. Our line parameter error models were derived while assuming no errors in the laser beam bearings.

It has been also found that errors in the estimated line parameters can have a substantial systematic error component. As we have shown the systematic error can be even larger than random errors. The sources of these errors have been identified as
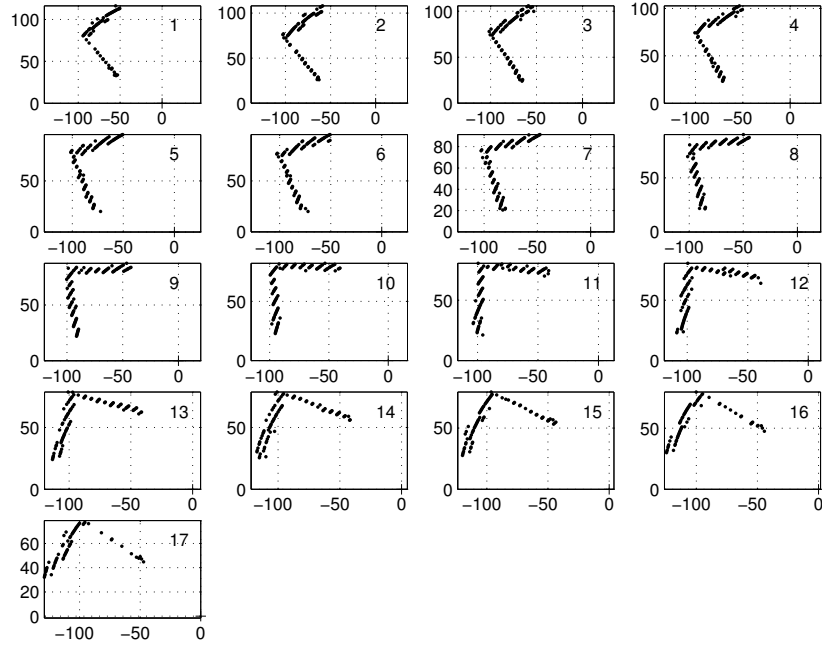
Figure 17: Samples of scans of corners in Cartesian coordinate system for the experiment where $R = 1.5m, \Delta\Theta = 5°$. Laser scanner position are depicted as a '+'.
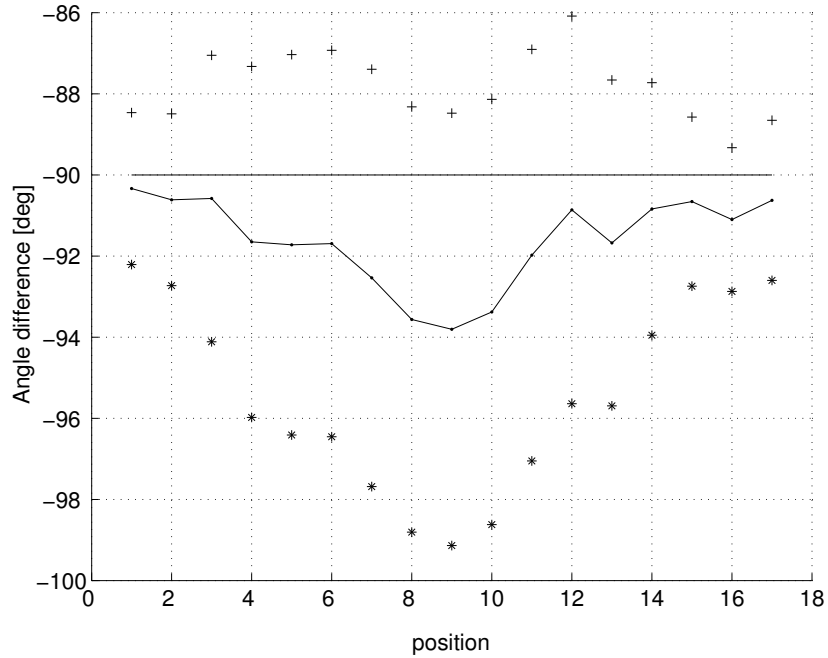

Figure 18: Systematic error model test ($R = 1.5m, \Delta\Theta = 5°$): measured opening angle of a right angle corner and error upper and lower bound estimates.
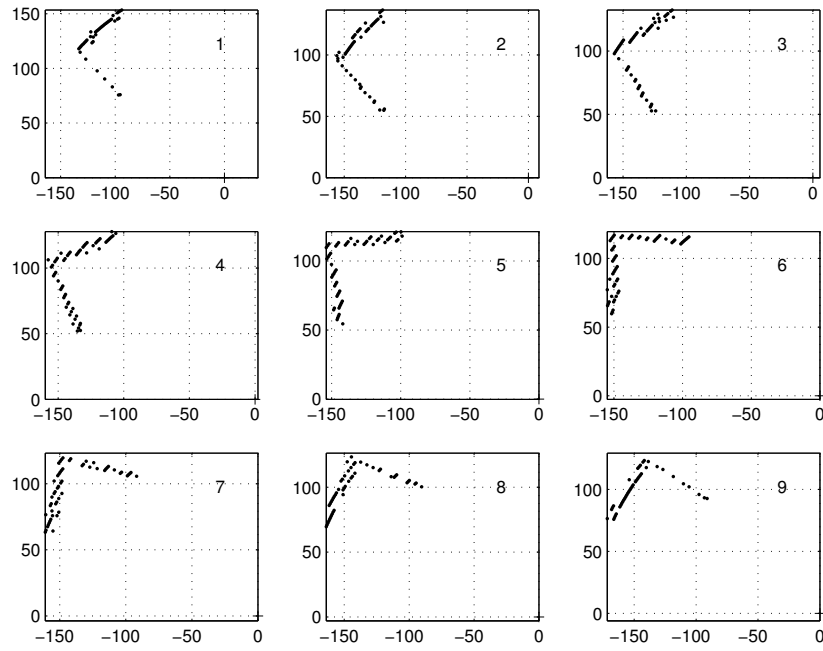
Figure 19: Samples of scans of corners in Cartesian coordinate system for the experiment where $R = 2m, \Delta\Theta = 10°$. Laser scanner position are depicted as a '+'.

Figure 20: Systematic error model test ($R = 2m, \Delta\Theta = 10°$): measured opening angle of a right angle corner and error upper and lower bound estimates.

Figure 21: Samples of scans of corners in Cartesian coordinate system for the experiment where $R = 3m, \Delta\Theta = 5°$. Laser scanner position are depicted as a '+'.
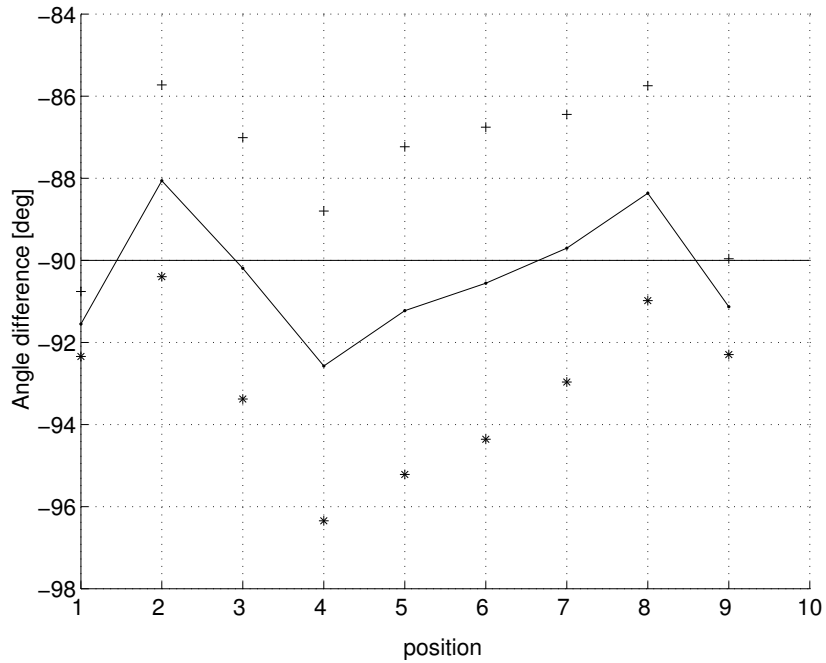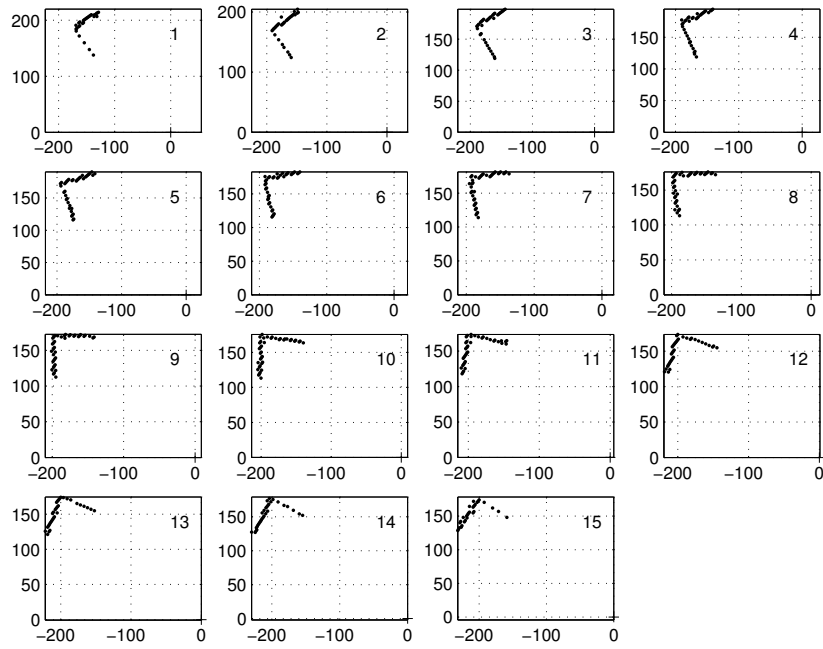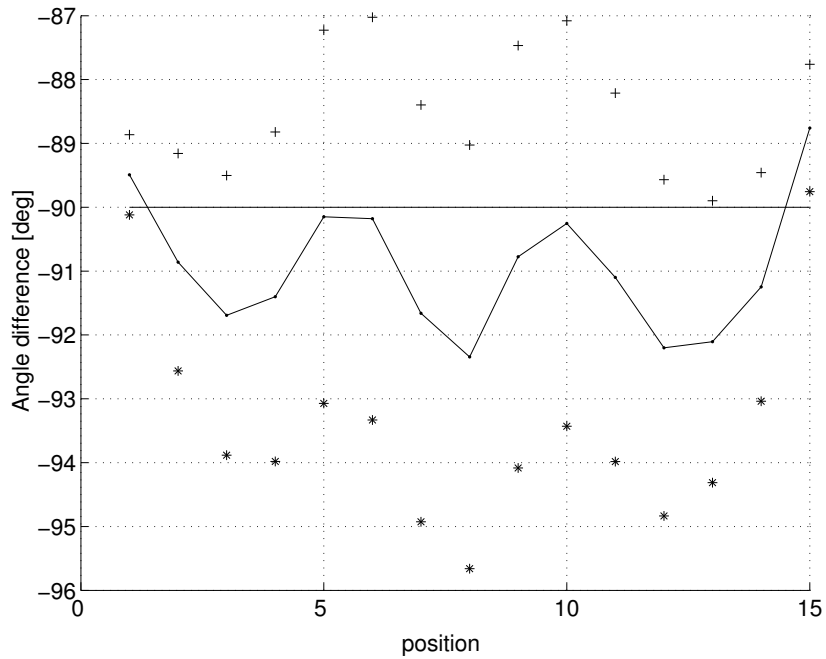

Figure 22: Systematic error model test ($R = 3m, \Delta\Theta = 5°$): measured opening angle of a right angle corner and error upper and lower bound estimates.

constant bias in the range measurements, bias changing linearly with range, bias depending on incidence angle and bias due to quantization. An attempt has been made to estimate worst-case systematic errors in line parameters. Experiments using a right angle corner have shown the model to be reasonably accurate but on rare occasions under-estimates the angle error. Systematic error estimates were not used for error compensation since we estimated the upper bound only.

The applicability of our systematic error models is restricted to laser scanners with a similar principle of operation as the Sick PLS. One example is the laser scanner described in [14]. Even if the whole systematic error model is not applicable to a particular laser scanner, parts of it could be used. For example, many lasers have a bias in their range readings which changes during warm-up.

In the future, we plan to test the new Sick LMS laser scanner. We also plan to work on the fusion of line parameters obtained from laser and sonar measurements.

5 Acknowledgments

A Derivations of Formulas

A.1 Line in Polar Coordinate System

If we substitute the equations for transformation of a point from polar to Cartesian frame

$$x = r \cos \phi \tag{117}$$

$$y = r \sin \phi \tag{118}$$

into the normal equation of a line:

$$x \cos(\alpha) + y \sin(\alpha) = d \tag{119}$$

we get

$$r \cos(\alpha) \cos(\phi) + r \sin(\alpha) \sin(\phi) = d \tag{120}$$

Which can be simplified to

$$r \cos(\alpha - \phi) = d \tag{121}$$

A.2 Conversion of Lines from Slope-Intercept Form to Normal Form

Line expressed in normal form:

$$x \cos \alpha + y \sin \alpha = d \tag{122}$$

Line expressed in slope-intercept form:

$$y = kx + q \tag{123}$$

36

Lets rewrite eq. 123 so, that the coefficients at coordinates x,y constitute a unit vector:

$$\frac{-k}{\sqrt{1+k^2}}x + \frac{1}{\sqrt{1+k^2}}y = \frac{q}{\sqrt{1+k^2}} \tag{124}$$

When comparing eq. 124 and eq. 122, it is clear, that they are equivalent only if:

$$\frac{-k}{\sqrt{1+k^2}} = \cos\alpha \tag{125}$$

$$\frac{1}{\sqrt{1+k^2}} = \sin\alpha \tag{126}$$

$$\frac{q}{\sqrt{1+k^2}} = d \tag{127}$$

Upon using eq. 126, α would be always bigger then 0 and smaller than $\pi/2$, because of the restricted domain of definition of inverse sinus. Therefore eq. 126 was used to determine α. However, the inverse of cosine returns values in the $< 0, \pi >$ interval, and d has to be bigger than 0, therefore the result has to be modified to get:

$$\alpha = \arccos\frac{-k}{\sqrt{1+k^2}} + (sign(q) - 1)\frac{\pi}{2} \tag{128}$$

$$d = \frac{|q|}{\sqrt{1+k^2}} \tag{129}$$

A.3 Line Fitting in Cartesian Coordinate System by Minimizing Perpendicular Distance

In [1] the authors show the solution of the line fitting problem in Cartesian coordinate system, by minimizing the weighted perpendicular distance of points to a line. They also show how to calculate the covariance of the estimated line parameters (α, d) depending on the noise in the range readings. However there are some minor details missing, therefore we will attempt to derive a covariance estimate for a simplified case while following a similar approach to theirs. In [1] the line parameter estimate is:

$$\tan 2\alpha = \frac{-2\sum w_i(\bar{y}_w - y_i)(\bar{x}_w - x_i)}{\sum w_i\left[(\bar{y}_w - y_i)^2 - (\bar{x}_w - x_i)^2\right]} \tag{130}$$

$$d = \bar{x}_w\cos\alpha + \bar{y}_w\sin\alpha \tag{131}$$

For computations, they recommend to use in eq. 130 the four quadrant arctangent.

For simplicity, we have derived the covariance estimate only for a special case of the previous equations where the weights are uniform:

$$\tan 2\alpha = \frac{-2\sum(\bar{y} - y_i)(\bar{x} - x_i)}{\sum\left[(\bar{y} - y_i)^2 - (\bar{x} - x_i)^2\right]} = \frac{N}{D} = f \tag{132}$$

$$d = \bar{x}\cos\alpha + \bar{y}\sin\alpha \tag{133}$$

Lets introduce $\mathbf{b}$ as $\mathbf{b} = [\alpha\ d]^T = g(\alpha, d)$. Then the first order Taylor expansion of $\mathbf{b}$ is:

$$\Delta\mathbf{b} = \nabla g(\mathbf{x}, \mathbf{y})\Delta\left[\mathbf{x}^T\ \mathbf{y}^T\right]^T = \mathbf{J}\Delta\left[\mathbf{x}^T\ \mathbf{y}^T\right]^T \tag{134}$$

where $\mathbf{J}$ is the Jacobian of eq.132-133. If the Jacobian is known, the covariance of (α, d) can be approximated as:

$$Cov(\alpha, d) = \mathbf{C_{\alpha,d}} = \mathbf{J C_{xy} J^T} \tag{135}$$

Elements of the Jacobian were calculated as following:

$$J_{j,1} = \frac{\partial \alpha}{\partial x_j} = \frac{1}{2} \frac{\partial \arctan(f)}{\partial f} \frac{\partial f}{\partial x_j} =$$

$$= \frac{1}{2} \frac{1}{1+f^2} \frac{\frac{\partial N}{\partial x_j} M - N \frac{\partial D}{\partial x_j}}{D^2} = \frac{(\bar{y} - y_j)D - (\bar{x} - x_j)N}{N^2 + D^2} \tag{136}$$

$$J_{n+j,1} = \frac{\partial \alpha}{\partial y_j} = \frac{1}{2} \frac{\partial \arctan(f)}{\partial f} \frac{\partial f}{\partial y_j} =$$

$$= \frac{1}{2} \frac{1}{1+f^2} \frac{\frac{\partial N}{\partial y_j} M - N \frac{\partial D}{\partial y_j}}{D^2} = \frac{(\bar{x} - x_j)D + (\bar{y} - y_j)N}{N^2 + D^2} \tag{137}$$

$$J_{j,2} = \frac{\partial d}{\partial x_j} = \frac{\partial \bar{x}}{\partial x_j} \cos \alpha + \bar{x} \frac{\partial \alpha}{\partial x_j} + \bar{y} \frac{\partial \sin \alpha}{\partial x_j} =$$

$$= \frac{1}{n} \cos \alpha + (\bar{y} \cos \alpha - \bar{x} \sin \alpha) \frac{\partial \alpha}{\partial x_j} \tag{138}$$

$$J_{n+j,2} = \frac{\partial d}{\partial y_j} = \bar{y} \frac{\partial \sin \alpha}{\partial y_j} + \frac{\partial \bar{y}}{\partial y_j} \sin \alpha + \bar{y} \frac{\partial \sin \alpha}{\partial y_j} =$$

$$= \frac{1}{n} \sin \alpha + (\bar{y} \cos \alpha - \bar{x} \sin \alpha) \frac{\partial \alpha}{\partial y_j} \tag{139}$$

where the following identities were used:

$$\frac{\partial \bar{x}}{\partial x_j} = \frac{1}{n} \frac{\partial \sum x_i}{\partial x_j} = \frac{1}{n} \tag{140}$$

$$\frac{\partial \bar{y}}{\partial y_j} = \frac{1}{n} \frac{\partial \sum y_i}{\partial y_j} = \frac{1}{n} \tag{141}$$

$$\frac{\partial N}{\partial x_j} = -2 \sum_i [(\bar{y} - y_i)(\bar{x} - x_i)] =$$

$$= -2 \left(\sum_{i \neq j} \frac{\bar{y} - y_i}{n} + (\bar{y} - y_j)(\frac{1}{n} - 1) \right) = 2(\bar{y} - y_j) \tag{142}$$

$$\frac{\partial N}{\partial y_j} = 2(\bar{x} - x_j) \tag{143}$$

$$\frac{\partial D}{\partial x_j} = \sum_i \frac{\partial}{\partial x_j} \left[(\bar{y} - y_i)^2 - (\bar{x} - x_i) \right]^2 =$$

$$= -2 \sum_{i \neq j} \frac{\bar{x} - x_i}{n} - 2(\bar{x} - x_j)(\frac{1}{n} - 1) = 2(\bar{x} - x_i) \tag{144}$$

$$\frac{\partial D}{\partial y_j} = -2(\bar{y} - y_i) \tag{145}$$

Calculating the covariance matrix of (α, d) directly from eq. 135 is not a good idea, because $\mathbf{C}_{xy}$ is of size $2n \times 2n$. However if the individual measurements are considered

38

to be independent then the covariance can be calculated as:

$$\mathbf{C}_{\alpha,\mathbf{d}} = \sum_i^n \mathbf{J_i C_{xyi} J_i^T} = \sum_i^n \begin{bmatrix} \frac{\partial \alpha}{\partial x_i} & \frac{\partial \alpha}{\partial y_i} \\ \frac{\partial d}{\partial x_i} & \frac{\partial d}{\partial y_i} \end{bmatrix} \mathbf{C_{xyi}} \begin{bmatrix} \frac{\partial \alpha}{\partial x_i} & \frac{\partial d}{\partial x_j} \\ \frac{\partial \alpha}{\partial y_i} & \frac{\partial d}{\partial y_i} \end{bmatrix} \tag{146}$$

where $\mathbf{C_{xy_i}}$ can be approximated after a first order Taylor expansion as:

$$\mathbf{C_{xyi}} = \begin{bmatrix} -r_i \sin \phi_i & \cos \phi_i \\ r_i \cos \phi_i & \sin \phi_i \end{bmatrix} \begin{bmatrix} \sigma_\phi^2 & 0 \\ 0 & \sigma_r^2 \end{bmatrix} \begin{bmatrix} -r_i \sin \phi_i & r_i \cos \phi_i \\ \cos \phi_i & \sin \phi_i \end{bmatrix} \tag{147}$$

Or the expanded form can be used:

$$\sigma_{xi}^2 = r_i^2 \sigma_\phi^2 \sin^2 \phi_i + \sigma_r^2 \cos^2 \phi_i \tag{148}$$

$$\sigma_{yi}^2 = r_i^2 \sigma_\phi^2 \cos^2 \phi_i + \sigma_r^2 \sin^2 \phi_i \tag{149}$$

$$\sigma_{xyi} = (\sigma_r^2 - r_i^2 \sigma_\phi^2) \sin \phi_i \cos \phi_i \tag{150}$$

A.4 Derivation of eq. 60–61

What we want to know is, how line parameters change if the true ranges of horizontal line are perturbed. Lets assume, we have a line with parameters (α, d). Then our line can be described as:

$$r_i = \frac{d}{\cos(\alpha - \phi_i)} \tag{151}$$

If we assume to have a horizontal line with the true parameters $(\alpha_0 = \frac{\pi}{2}, d_0)$ and if we linearize eq. 151 around (α_0, d_0) we get:

$$\xi_i = r_i - r_{0i} \approx \frac{\Delta d}{\sin \phi_i} + \frac{d_0 \cos \phi_i}{\sin^2 \phi_i} = a_i \Delta d + b_i \Delta \alpha \tag{152}$$

where $a_i = \frac{1}{\sin \phi_i}$ and $b_i = \frac{d_0 \cos \phi_i}{\sin^2 \phi_i}$.

We can interpret ξ_i as the range difference we get if we add $(\Delta \alpha, \Delta d)$ to (α_0, d_0). Therefore if we know that a bias of ξ_{mi} is added to each true range, then we can get an estimate of $\Delta \alpha, \Delta d$ if we minimize sum of square deviations between the bias ξ_{mi} and the estimated range difference ξ_i:

$$E = \sum (\xi_i - \xi_{mi})^2 = \sum (a_i \Delta d + b_i \Delta \alpha - \xi_{mi})^2 \tag{153}$$

To find $\Delta \alpha, \Delta d$ which minimize E, we need to differentiate eq. 153 with respect to $\Delta \alpha$ and Δd, and find out where are they equal to 0:

$$\frac{\partial E}{\partial \Delta \alpha} = 2 \sum (a_i \Delta d + b_i \Delta \alpha - \xi_{mi}) a_i = 0 \tag{154}$$

$$\frac{\partial E}{\partial \Delta d} = 2 \sum (a_i \Delta d + b_i \Delta \alpha - \xi_{mi}) b_i = 0 \tag{155}$$

Expanding the previous equations and dividing by 2 results in:

$$\Delta d \sum a_i^2 + \Delta \alpha \sum b_i a_i = \sum \xi_{mi} a_i \tag{156}$$

$$\Delta d \sum a_i b_i + \Delta \alpha \sum b_i^2 = \sum \xi_{mi} b_i \tag{157}$$

of which solution is:

$$\Delta\alpha = \frac{\sum \xi_{mi} a_i \sum a_i b_i - \sum \xi_{mi} b_i \sum a_i^2}{\left(\sum b_i a_i\right)^2 - \sum b_i^2 \sum a_i^2} \tag{158}$$

$$\Delta d = \frac{\sum \xi_{mi} b_i \sum a_i b_i - \sum \xi_{mi} a_i \sum b_i^2}{\left(\sum b_i a_i\right)^2 - \sum b_i^2 \sum a_i^2} \tag{159}$$

The last two equations are special case of the approach shown in section 2.3 for estimating lines in polar coordinate system. The difference is that only one iteration is made (small range deviations are assumed) and the true line must be horizontal.

B More Experimental Results

B.1 Covariance and Correlation Coefficient Matrices of Range Readings

To support our assumption, that estimating the range measurement covariance matrix as a diagonal matrix is sufficient, we show the first 7x7 sub-matrices of the covariance and correlation coefficient matrices of range readings for line 1 and 13 (see fig. 9). All matrices in graphical representation are shown on fig. 7. For the calculation of these matrices, about 3000 samples were used.

$$cov_1 = \begin{bmatrix} 3.502 & 0.385 & -0.016 & 0.242 & 0.173 & 0.001 & 0.364 \\ 0.385 & 4.704 & -0.051 & 0.266 & 0.673 & 0.200 & 0.367 \\ -0.016 & -0.051 & 5.335 & 1.080 & 0.422 & 0.471 & 0.235 \\ 0.242 & 0.266 & 1.080 & 6.186 & 1.232 & 0.253 & 0.558 \\ 0.173 & 0.673 & 0.422 & 1.232 & 7.357 & 1.308 & 0.769 \\ 0.001 & 0.200 & 0.471 & 0.253 & 1.308 & 8.809 & 0.528 \\ 0.364 & 0.367 & 0.235 & 0.558 & 0.769 & 0.528 & 7.954 \end{bmatrix} \tag{160}$$

$$corr_1 = \begin{bmatrix} 1.000 & 0.095 & -0.004 & 0.052 & 0.034 & 0.000 & 0.069 \\ 0.095 & 1.000 & -0.010 & 0.049 & 0.114 & 0.031 & 0.060 \\ -0.004 & -0.010 & 1.000 & 0.188 & 0.067 & 0.069 & 0.036 \\ 0.052 & 0.049 & 0.188 & 1.000 & 0.183 & 0.034 & 0.079 \\ 0.034 & 0.114 & 0.067 & 0.183 & 1.000 & 0.163 & 0.101 \\ 0.000 & 0.031 & 0.069 & 0.034 & 0.163 & 1.000 & 0.063 \\ 0.069 & 0.060 & 0.036 & 0.079 & 0.101 & 0.063 & 1.000 \end{bmatrix} \tag{161}$$

$$cov_{13} = \begin{bmatrix} 6.008 & 0.062 & -0.003 & -0.576 & 0.145 & -0.165 & 0.344 \\ 0.062 & 2.430 & 0.242 & 0.293 & 0.119 & 0.211 & 0.066 \\ -0.003 & 0.242 & 4.128 & 0.272 & -0.042 & 0.124 & 0.034 \\ -0.576 & 0.293 & 0.272 & 6.329 & 0.216 & 0.131 & -0.086 \\ 0.145 & 0.119 & -0.042 & 0.216 & 2.579 & 0.077 & 0.140 \\ -0.165 & 0.211 & 0.124 & 0.131 & 0.077 & 5.362 & 0.343 \\ 0.344 & 0.066 & 0.034 & -0.086 & 0.140 & 0.343 & 5.562 \end{bmatrix} \tag{162}$$

$$corr_{13} = \begin{bmatrix} 1.000 & 0.016 & -0.001 & -0.093 & 0.037 & -0.029 & 0.060 \\ 0.016 & 1.000 & 0.076 & 0.075 & 0.048 & 0.058 & 0.018 \\ -0.001 & 0.076 & 1.000 & 0.053 & -0.013 & 0.026 & 0.007 \\ -0.093 & 0.075 & 0.053 & 1.000 & 0.054 & 0.022 & -0.014 \\ 0.037 & 0.048 & -0.013 & 0.054 & 1.000 & 0.021 & 0.037 \\ -0.029 & 0.058 & 0.026 & 0.022 & 0.021 & 1.000 & 0.063 \\ 0.060 & 0.018 & 0.007 & -0.014 & 0.037 & 0.063 & 1.000 \end{bmatrix} \quad (163)$$

As it can be seen from eq. 161,163, the correlation coefficients are most of the time quite small.

References

[1] K. O. Arras and R. Siegwart. Feature extraction and scene interpretation for map-based navigation and map building. In *Proceedings of SPIE, Mobile Robotics XII*, volume 3210, 1997.

[2] M. K. Brown. On quantization of noisy signals. *IEEE Transactions on Signal Processing*, 39:836–841, April 1991.

[3] R. Deriche, R. Vaillant, and O. Faugeras. *From Noisy Edges Points to 3D Reconstruction of a Scene : A Robust Approach and Its Uncertainty Analysis*, volume 2, pages 71–79. World Scientific, 1992. Series in Machine Perception and Artificial Intelligence.

[4] Erwin Sick GmbH. *Opearating Instructions, PLS and PLS User Software Laser Scanner*. Waldkirch.

[5] J.-S. Gutmann. *Robuste Navigation autonomer mobiler Systeme*. PhD thesis, Albert-Ludwigs-Universität Freiburg, 2000.

[6] Martial Hebert. Active and passive range sensing for robotics. In *Proceedings of the 2000 IEEE International Conference on Robotics and Automation*, pages 102–110, San Francisco, CA, April 2000. IEEE.

[7] A. Jeffrey. *Handbook of Mathematical Formulas and Integrals*. Academic Press, London, second edition, 2000.

[8] P. Jensfelt. *Approaches to Mobile Robot Localization in Indoor Environments*. PhD thesis, KTH, 2001.

[9] Steven M. Kay. *Fundamentals of Statistical Signal Processing*, volume 2. Estimation Theory. Prentice Hall, New Jersey, 1993.

[10] L. Kleeman. On-the-fly classifying sonar with accurate range and bearing estimation. In *IEEE/RSJ International Conference on Intelligent Robots and Systems*, pages 178–183. IEEE, 2002.

[11] J. Nygårds. *On Robot Feedback from Range Sensors: Reliable Control by Active Reduction of Uncertainty and Ambiguities*. PhD thesis, Lindköping University, 1998.

[12] R. P. Paul. *Robot manipulators : mathematics, programming, and control : the computer control of robot manipulators*. MIT Press, Cambridge, Mass., 1981.

[13] S. T. Pfister, K. L. Kriechbaum, S. I. Roumeliotis, and J. W. Burdick. Weighted range sensor matching algorithms for mobile robot displacement estimation. In *Proceedings of the IEEE International Conference on Robotics and Automation*, Washington D.C., May 2002. IEEE.

[14] Antonio Reina and Javier Gonzales. Characterization of a radial laser scanner for mobile robot navigation. In *IROS'97*, pages 579–585. IEEE, 1997.

[15] R. M. Taylor and P. J. Probert. Range finding and feature extraction by segmentation of images for mobile robot navigation. In *Proceedings of the 1996 IEEE International Conference on Robotics and Automation*, pages 95–100, Minneapolis, Minnesota, April 1996. IEEE.

[16] G. B. Wetherill. *Regression analysis with applications*. Chapman and Hall, London, 1986.

[17] H. Wetteborn. Laserabstandsermittlungsvorrichtung, 1993. German patent no. DE4340756A1 (November 30, 1993).

[18] C. Ye and J. Borenstein. Characterization of a 2-d laser scanner for mobile robot obstacle negotiation. In *Proceedings of the 2002 IEEE International Conference on Robotics and Automation*, pages 2512–2518, Washington DC, May 2002. IEEE.